Science of the Total Environment 870 (2023) 161887

Contents lists available at ScienceDirect

Science of the Total Environment

journal homepage: www.elsevier.com/locate/scitotenv

Iron inactivation by *Sporobolomyces ruberrimus* and its potential role in plant metal stress protection. An *in vitro* study

Roman J. Jędrzejczyk [a,*], Maciej Gustab [a], Rafał Ważny [a], Agnieszka Domka [j], Przemysław J. Jodłowski [b], Maciej Sitarz [c], Patryk Bezkosty [c], Michał Kowalski [a], Dominika Pawcenis [d], Kinga Jarosz [e], Victor Sebastian [f,g,h,i], Paweł P. Łabaj [a], Piotr Rozpądek [a,*]

[a] Małopolska Centre of Biotechnology, Jagiellonian University, Gronostajowa 7A, 30-387 Kraków, Poland
[b] Faculty of Chemical Engineering and Technology, Cracow University of Technology, Warszawska 24, 30-155 Kraków, Poland
[c] Faculty of Materials Science and Ceramics, AGH University of Science and Technology, Mickiewicza 30, 30-059 Kraków, Poland
[d] Faculty of Chemistry, Jagiellonian University, Gronostajowa 2, 30-387 Kraków, Poland
[e] Institute of Geological Sciences, Jagiellonian University, Gronostajowa 3a, 30-387 Kraków, Poland
[f] Instituto de Nanociencia y Materiales de Aragón (INMA), CSIC-Universidad de Zaragoza, Zaragoza, Spain
[g] Department of Chemical and Environmental Engineering, Universidad de Zaragoza, Campus Rio Ebro, 50018 Zaragoza, Spain
[h] Networking Research Center on Bioengineering, Biomaterials and Nanomedicine (CIBER-BBN), 28029 Madrid, Spain
[i] Laboratorio de Microscopías Avanzadas, Universidad de Zaragoza, 50018 Zaragoza, Spain
[j] W. Szafer Institute of Botany Polish Academy of Sciences, Lubicz 46, 31-512 Kraków, Poland

HIGHLIGHTS

- *S. ruberrimus* facilitates *A. arenosa* growth in sterile metal enriched medium.
- *S. ruberrimus* is capable of precipitating Fe deposits.
- *A. arenosa* cocultered with the yeast for 10 days exhibited less stress symptoms.

GRAPHICAL ABSTRACT

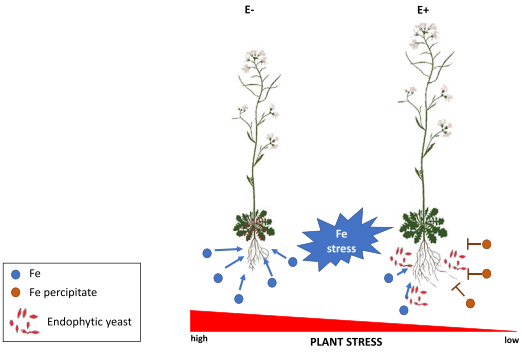

ARTICLE INFO

Editor: Charlotte Poschenrieder

Keywords:
Arabidopsis arenosa
Toxic metals
iron inactivation

ABSTRACT

The endophytic Basidiomycete *Sporobolomyces ruberrimus* protects its host *Arabidopsis arenosa* against metal toxicity. Plants inoculated with the fungus yielded more biomass and exhibited significantly fewer stress symptoms in medium mimicking mine dump conditions (medium supplemented with excess of Fe, Zn and Cd). Aside from fine-tuning plant metal homeostasis, the fungus was capable of precipitating Fe in the medium, most likely limiting host exposure to metal toxicity. The precipitated residue was identified by Fourier transform infrared spectroscopy (FTIR), X-ray photoelectron spectroscopy (XPS), X-Ray Diffraction (XRD) and electron microscopy (SEM/TEM) with energy dispersive X-Ray analysis (EDX/SAED) techniques. The performed analyses revealed that the fungus transforms iron into amorphous (oxy)hydroxides and phosphates and immobilizes them in the form of a precipitate changing Fe behaviour in the MSR medium. Moreover, the complexation of free Fe ions by fungi could be obtained by biomolecules such as lipids, proteins, or biosynthesized redox-active molecules.

* Corresponding authors.
E-mail addresses: roman.jedrzejczyk@uj.edu.pl (R.J. Jędrzejczyk), maciej.gustab@doctoral.uj.edu.pl (M. Gustab), rafal.wazny@uj.edu.pl (R. Ważny), agnieszka.domka@uj.edu.pl (A. Domka), przemyslaw.jodlowski@pk.edu.pl (P.J. Jodłowski), msitarz@agh.edu.pl (M. Sitarz), bezkosty@agh.edu.pl (P. Bezkosty), m.kowalski@doctoral.uj.edu.pl (M. Kowalski), d.pawcenis@uj.edu.pl (D. Pawcenis), kinga.borek@uj.edu.pl (K. Jarosz), pawel.labaj@uj.edu.pl (P.P. Łabaj), piotr.rozpadek@uj.edu.pl (P. Rozpądek).

http://dx.doi.org/10.1016/j.scitotenv.2023.161887
Received 2 August 2022; Received in revised form 18 January 2023; Accepted 25 January 2023
Available online 30 January 2023

1. Introduction

The demand for metals such as lithium, cobalt, zinc, and nickel for the industry has a significant impact on ecosystem functioning. This threat will become even more dangerous due to the gradual increase in the intensity of exploitation of Co and Ni deposits. The semiconductive and catalytic properties of these metals are being utilized in energy storage (Gao et al., 2009; Kumar et al., 2019; Li et al., 2020), electronics (Jing et al., 2021), and the catalysts production (Rueda et al., 2021). These elements are obtained from ores that are extracted through different mining procedures, which generate wastes that are an uneconomic or have a contaminated fraction. Postmining wastes are usually enriched with large quantities of accompanying, potentially toxic, metals and metalloids such as iron, arsenic and copper. Toxic metal (TM)-enriched substrates are usually stored as mine dumps and exposed to oxidation or weathering as a source of environmental pollution. Therefore, postmining wastes that contain potentially toxic elements in large abundance are a considerable problem for public health, agriculture and the economy (Mudd et al., 2017). Toxic metals that can be taken up by plant are a severe threat to the plant and a dangerous route of metal input into the food chain. Thus, strategies aiming to reduce the deleterious effects of TM are currently needed. On the other hand, some metals (Fe, Zn, Mo) are micro- or macronutrients for plants and other multicellular organisms. They are building blocks of essential molecules, such as enzymes and other proteins, that are required for proper functioning; thus, a tightly regulated mechanism of metal uptake and detoxification is necessary for optimizing growth and development. Iron, for example, is a crucial component of haem proteins such as cytochromes, catalase and ferredoxin (Coon, 1980), but its excess is undesirable. Reductions in the yield of the world's leading crop species, wheat and rice reaching up to 100 %, make iron pollution one of the most formidable crop management and research challenges (Sahrawat, 2004). Nevertheless, plants can cope with elevated concentrations of metals in soil by utilizing different strategies. One is the plant's avoidance (exclusion) of heavy metals, which is associated with mechanisms for metal ion homeostasis and tolerance, including Fe homeostasis (Clemens, 2001). However, this strategy is not always fully effective due to the imperfect specificity of the nutrient uptake system. This imperfection causes heavy metals to enter the plant and subsequently poison it. This low specificity is caused by the character of metal transporters, which can chelate (bind) more than one type of ion. Due to the similarity of some toxic metal ions to nutrients, transporters have a similar affinity for both.

In some cases, iron, as an active redox metal, can cause a specific plant response (Blute et al., 2004; Khan et al., 2016). This redox character is associated mainly with Fe^{2+}/Fe^{3+} equilibrium in wetland sediment systems, where iron is ubiquitous. It must be emphasized that in anoxic sediment pore water, ferrous ions are the dominant iron species and an active electron donor. On the other hand, in oxygen-rich waters, ferric ions are the dominant iron species – the equilibrium is then associated with the reaction: $Fe^{3+} + e^{-} \rightarrow Fe^{2+}$. The Fe^{2+} ion in the rhizosphere is oxidized by the root-released O_2. This causes oxidized ions (Fe^{3+}) to precipitate and accumulate as iron plaques on hydrophytic root surfaces in the form of orange iron oxyhydroxide (FeOOH) (Khan et al., 2016; St-Cyr et al., 1993) ferric hydroxide (Crowder and Macfie, 1986; Emerson et al., 1999) ferrihydrite (Peng et al., 2018) and other morphologically varied Fe compounds. These precipitates can exhibit crystalline and amorphous nature depending on the type of chemical compounds and their interaction with ligands. This ability was shown to be characteristic of wetland monocots. Because iron oxides can strongly adsorb divalent metallic cations such as Zn^{2+} and Cd^{2+}; they play a crucial role in the cycling of heavy metals in the environment and affect metal bioavailability and mobility in the medium. Compounds deposited on roots as a result of the formation of iron plaque are also a reservoir of nutrients because, similar to metal ions, nutrients can be adsorbed by the deposits (Zheng et al., 2012).

Plants interact with a wide array of microorganisms that inhabit the surrounding environment. One group includes mutualistic and commensal microorganisms that in many cases facilitate plant adaptation to the environment, including adaptation to metal toxicity. Recent reports clearly show the significance of the microbe component in the metabolism of the holobiont (Bilal et al., 2019; Rozpądek et al., 2018; Ważny et al., 2018, 2021a). An important aspect of plant-microorganism interactions and adaptation to the environment is the ability of symbiotic microorganisms to synthesize active compounds. Chemical individual such as metal nanoparticles and organic acids (Li et al., 2019) sequester xenobiotics and detoxify them, providing plants and other organisms with the protection necessary for growth and development in often highly polluted environments. This has a significant impact on the entire soil system.

Our investigations (Domka et al., 2023) showed that the endophytic yeast *Sporobolomyces ruberrimus* isolated from a serpentine population of *Arabidopsis arenosa* protected plants against metal toxicity. We showed that plants grown in Pb-Zn dump substrate and in MSR medium supplemented with Zn, Cd and Fe yielded more biomass than not inoculated plants and exhibited less metal stress symptoms. An important aspect of microorganism dependent adaptation to metal toxicity was the inhibition of host Fe uptake. Lower Fe concentrations were found in both roots and shoots of plants cocultered with the fungus. The microorganism did not affect Zn or Cd take up by the plant, nor did inoculated plants yield more biomass when cultured in medium supplemented with a Zn or Cd alone. One aspect of the metal uptake inhibition conferred by the fungus was optimizing the plant related metal uptake and the plant metal sensing network.

In this study we hypothesized that in addition to optimizing plant Fe uptake under metal excess as shown in Domka et al. (2023), the fungus was capable of lowering Fe bioavailability and mobility in medium, preventing its uptake by plants. We show that plant metal uptake inhibition may also be related to the ability of symbiotic microorganisms to transform metals in the medium making it unavailable for plant uptake and thus protecting the plant from metal toxicity. The transcriptome of *Arabidopsis arenosa* inoculated with the fungus clearly showed that the plant stress response under metal toxicity was downregulated. We characterized the metal deposit precipitated by the microorganism *in vitro*. The results of the investigations presented in this study describe the complex network of interactions between plants, microorganisms and the environment and show the importance of plant-microorganism interactions in ecosystem functioning and its possible role in the remediation of metal-polluted environments.

2. Experimental

2.1. Experimental design

A schematic representation of the experimental design is presented in Fig. 1. To evaluate the role of the endophytic yeast in plant metal tolerance three independent experimental approaches were utilized. In this paragraph only the aims of these experiments were described. The analytical methods were described in Sections 2.2–2.20. *Arabidopsis arenosa*was cultured in medium supplemented with toxic metals or mine dump soil in the following experimental setup: “TM + E − ” - medium supplemented with toxic metals, plant not inoculated with fungus and “TM + E + ” - medium supplemented with toxic metals, plant inoculated with fungus. If necessary “TM-E − ” (medium not supplemented with toxic metals, plants not inoculated with fungus) as the negative control for experiments was used. The “n” number describes the number of biological repetitions, not technical repetitions.

Experimental setup 1. Plant/soil mine dump experiment

The aim of this series of experiments was to show how *S. ruberrimus* associated with *A. arenosa* facilitates plant adaptation to metal toxicity. *A. arenosa* was cultured in mine dump substrate mixed with sand in 1:1 (v/v) ratio, one experimental group of plants was inoculated with *S. ruberrimus* (TM + E +), while the control group was not (TM + E −) – the details can be find in Section 2.4. To verify the stress protective role of the microorganism described in Domka et al. (2023) plant fresh plant biomass was measured. For the characterization of soil in terms of mineralogical composition, XRD and SEM-EDS analyses were performed. Also the

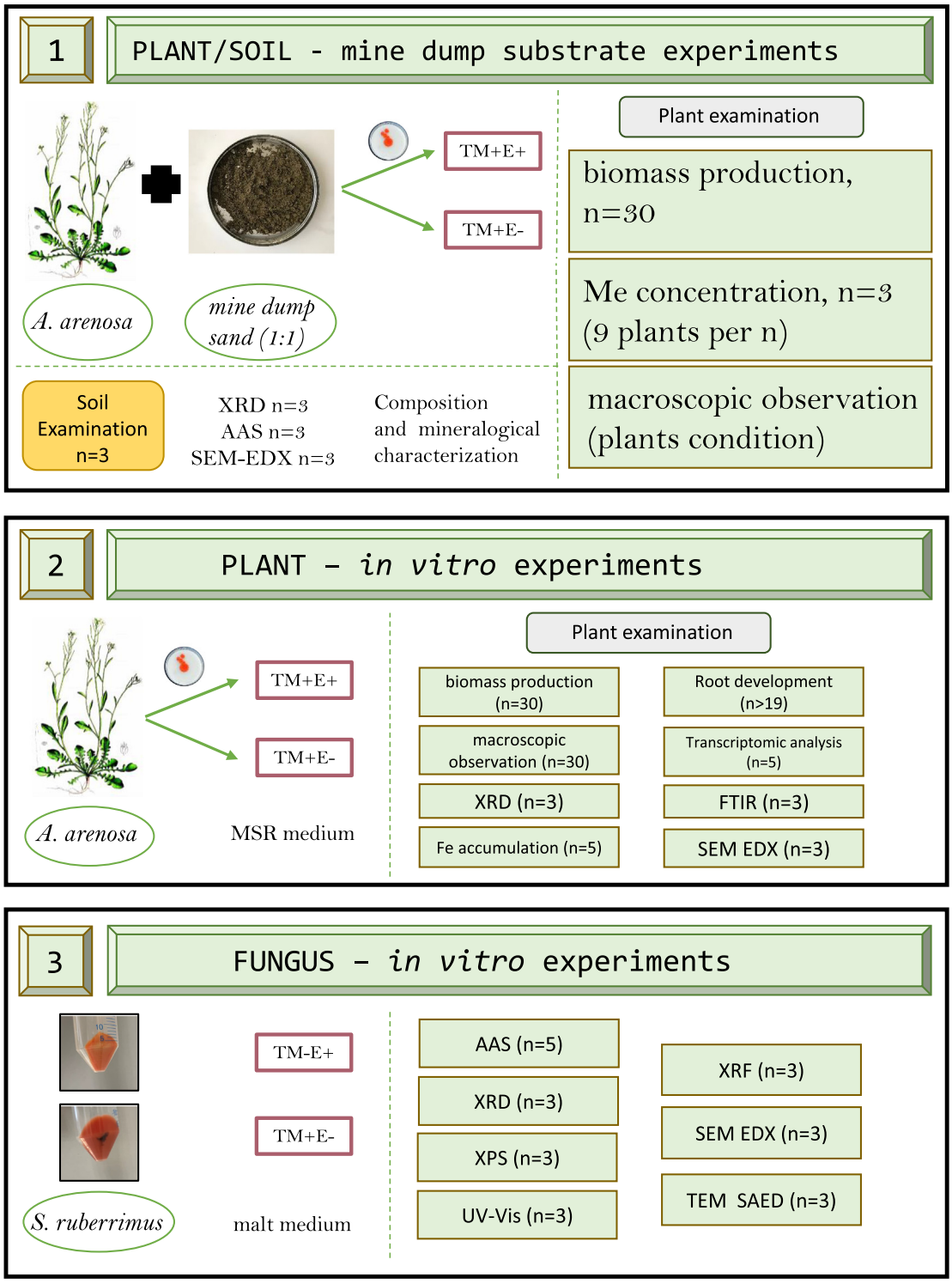

Fig. 1. Scheme of the experimental design with the list of analytical techniques used. For each analysis the biological (independent experiments) repetitions were marked.

comparison of rhizosphere and bulk soil were carried out to find the differences of Fe species. The number of biological replicates (n number) is indicated for each technique in the Fig. 1.

Experimental setup 2. Plant-yeast *in vitro* coculture

The aim of the experiments was to verify the effect of the fungus on plant adaptation to elevated concentration of toxic metals, especially Fe. Plants were cultured in MSR medium, with and without supplementation with toxic metals. One group of plants was inoculated with *S. ruberrimus* and the other not. Biomass production, macroscopic observation (sublethal dose determination), Fe uptake by AAS, root architecture analysis, XRD, SEM-EDX, and RNAseq analysis were performed. To describe potential structural changes of plants which are inoculated with *S. ruberrimus* ATR-FTIR analysis was performed. The plants were cocultured in the *in vitro* system. Three experimental variants were tested. One is control (TM − E −) – *A. arenosa* cultured in MSR medium, TM + E + variant - *A. arenosa* inoculated with *S. ruberrimus* and cultured in MSR medium supplemented with Fe, Cd, and Zn, TM + E − variant - *A. arenosa* cultured in the MSR medium

Table 1
(Experiment 1). Concentration of metals in the "Bolesław" mine dump.

	Fe	Zn	Cd
"Bolesław" mind dump soil Concentration [mg kg^{-1}]	$(4.68 \pm 0.27)\cdot 10^4$	16,368 ± 577	100 ± 4.78
MSR medium after optimisation Concentration [μM]	458	448	2.22

supplemented with Fe, Cd and Zn without fungus. The FTIR analysis was performed for the plant-fungus consortium.

Experiment 3. Fungus – *in vitro* examination

The aim of the experiment was to verify if the endophytic fungus was capable of precipitating excess Fe in medium and likely immobilizing it, making it unavailable to the plant and thus lowering plant exposure to metal toxicity. In order to simplify of the model, we performed the experiment in the *in vitro* setup. The fungus was cultured in a liquid medium, 2 % malt extract medium supplemented with (TM+) and control - malt extract not supplemented with TM. The precipitated residue was characterized with XPS, XRF, FAAS, UV–Vis, XRD, SEM-EDX, and TEM SAED analyses. Three independent replicates for each analysis were performed. The number of biological replicates (n number) is indicated for each technique in the Fig. 1.

2.2. Fungus identification

Endophytic fungi were isolated from *Arabidopsis arenosa* (roots, shoots and flowers separately). Plants were collected from serpentine area in Sankt Marien-Feistritz, Austria (47.2834N, 14.9322E). Plant tissues were surface sterilized according to the following protocol: 1.5 % sodium hypochloride (with a drop of Tween) for 3 min, followed by rinsing in deionized water for 2 min and 75 % ethanol for 90 s and rinsing in deionized water for 1 min, 5 min and 1 min. The surface sterilized flowers were dried on a sterile paper filter, and placed on solid PDA (potato dextrose agar) droplets supplemented with antibiotics (200 mg·L^{-1} Streptomycin, 200 mg·L^{-1} Ampicillin, and 100 mg·L^{-1} Tetracycline). Plant fragments were incubated in the dark at 26 °C and inspected every day for 2 weeks. Emerging cultures were sequentially passaged to new PDA media.

The yeast strain used in this study was identified based on the sequence of the internal transcribed spacer of the fungal 1, the 5.8S rRNA gene, the internal transcribed spacer 2 and the large subunit rDNA region (ITS-LSU). DNA was extracted using cetyltrimethylammonium bromide (CTAB) according to Azmat et al. (2012) with modification by Domka et al. (2019). The concentration and purity of DNA were determined spectrophotometrically. The ITS-LSU rDNA region was amplified with ITS1F (Gardes and Bruns, 1993) and LR5 primers (Vilgalys and Hester, 1990). Polymerase chain reaction (PCR) was performed in 25μL reaction mixture containing 10 ng of DNA matrix, 9.5 μL of nuclease-free water, 12.5 μL of DreamTaq HS Green PCR Master Mix (Thermo Scientific, US), and 1 μL of each of the primers at a 10 pmol concentration for each sample. The EPPiC Fast kit (A&A Biotechnology, PL) was used for purification of the PCR products. The PCR products were sequenced by Macrogen Europe Laboratory (NL) using ITS1F and LR5 primers. The sequences were edited using Geneious Prime (www.geneious.com) and compared with sequences published in the NCBI (National Centre for Biotechnology Information) database (www.ncbi.nlm.nih.gov) using the BLASTn algorithm.

The nucleotide sequence of the yeast *S. ruberrimus* strain UNIJAG.PL.OP177 was deposited in GenBank under accession number ON331994 (Domka et al., 2023). Pure culture of the yeast species was deposited in the culture collection of the Institute of Agricultural and Food Biotechnology (IAFB) in Poland belonging to the World Data Centre under accession number KKP2090p.

2.3. Determination of metal concentration in soils

Soil metal concentrations were determined according to Melaku et al. (2005) with modifications. Briefly, the soil was dried at 105 °C, sieved through a 2 mm mesh, transferred quantitatively (2 g) into a test tube, aliquoted with 10 mL of aqua regia, and maintained at room temperature overnight. The soil was digested at 250 °C for 2 h. The suspension was then filtered and made up to 25 mL with deionized water. FAAS was used for determination of metal concentration. The results are presented in Table 1.

2.4. Plant cultivation – dump medium experiments

Arabidopsis arenosa seeds (mine dump, TM adapted population) were surface sterilized according to the following scheme: 4 min – 4 % NaOCl; 2 min – 96 % C_2H_5OH, 4 min – 75 % C_2H_5OH, 3× sterile ddH_2O. Sterile seeds were sown into sterile mixture of sand and soil at 1:1 ratio and incubated at 4 °C for 48 h, then pot was transferred to a growth chamber (Percival Scientific, US). After 14 days, seedlings were transferred to 50-mL pots filled with a sterile mixture of substrate from the "Bolesław" mine dump with sand at a 1:1 ratio and inoculated with *S. ruberrimus* by adding a yeast suspension with an optical density of 2.14 at 600 nm. After 20 days, the plants were harvested rinsed with deionized water and weighed with analytical precision. The photographs of plants and the biomas are presented in Fig. 2a. Three experiments were performed, 10 plants per "n" (Melaku et al., 2005).

2.5. Plant cultivation – in vitro experiments

Arabidopsis arenosa seeds (mine dump, TM adapted population) were surface sterilized as described in previous Section 2.4. Following sterilization, seeds were transferred to 1/4 MS medium (Murashige & Skoog Medium, Basal Salt Mixture [Duchefa Biochemie, Netherlands] – 1.074 g·L^{-1}, sucrose – 7.5 g·L^{-1}, Phytoagtar – 6 g·L^{-1}) and placed in a refrigerator at 4 °C for 48 h. Petri dishes with seeds were transferred to a cultivation chamber (Panasonic MLR-352H-PE, Korea with a 16 h photoperiod, under 100 μmol·m^{-2}·s^{-1} of light intensity, 21/17 °C day/night temperature and 50 % humidity) for 7 days. After germination, plants were transferred to square petri dishes with MSR (Strullu-Romand Medium [Duchefa Biochemie, Netherlands] – 0.594 g·L^{-1}, Ca$(NO_3)_2$·$4H_2O$ – 0.256 g·L^{-1}, Phytoagar – 6 g·L^{-1}) supplemented with metal ions (if applicable): Zn – 459 μM, Fe – 448 μM, Cd – 2.22 μM (0.0025B) and placed into a plant cultivation chamber under the same light conditions for 10 days. Photographs and biomass results of the plants are shown in Fig. 2b.

2.6. Determination of sublethal doses of metals

Arabidopsis arenosa was cocultured with *S. ruberrimus* in MSR medium supplemented with toxic metals (TM) designed to mimic the mine dump

Fig. 2. (Experiments 1 and 2). Stress protective effect of plant inoculation with *S. ruberrimus*: (a–b) the phenotype and fresh weight of *A. arenosa*: a) grown in substrate polluted with Fe (III), Zn(II), Cd(II) (TM+) from the mine dump "Bolesław" for 20 days, inoculated (E+) and not inoculated (E−) (n = 30), b) cultured *in vitro* on medium supplemented with Fe(III), Zn(II), Cd(II) (TM+) for 10 days, inoculated (E+) and not inoculated (E−) with *S. ruberrimus* (n = 30); c–d) the influence of *S. ruberrimus* on *A. arenosa* root growth parameters: root length (c) and number of lateral roots (d) under elevated concentrations of toxic metals (TM+). Plants were cultured *in vitro* in medium supplemented with TM for 10 days, inoculated (E+) and not inoculated (E−) with endophyte (n = 19); e) microscopic images of roots of plants cultured *in vitro* in medium with TM, inoculated (E+) and not inoculated (E−) with *S. ruberrimus*; f) Iron concentration in whole plants inoculated (E+) and not inoculated (E−) with *S. ruberrimus* (n = 3). Plants were cultured *in vitro* on medium supplemented with Fe(III), Zn(II), Cd(II) (TM+) for 10 days, inoculated (E+) and not inoculated (E−) with *S. ruberrimus* (n = 5). Stars indicate significant differences (*t*-test, * - $p \le 0.05$, ** - - $p \le 0.01$, *** - - $p \le 0.005$) between E+ and E− plants.

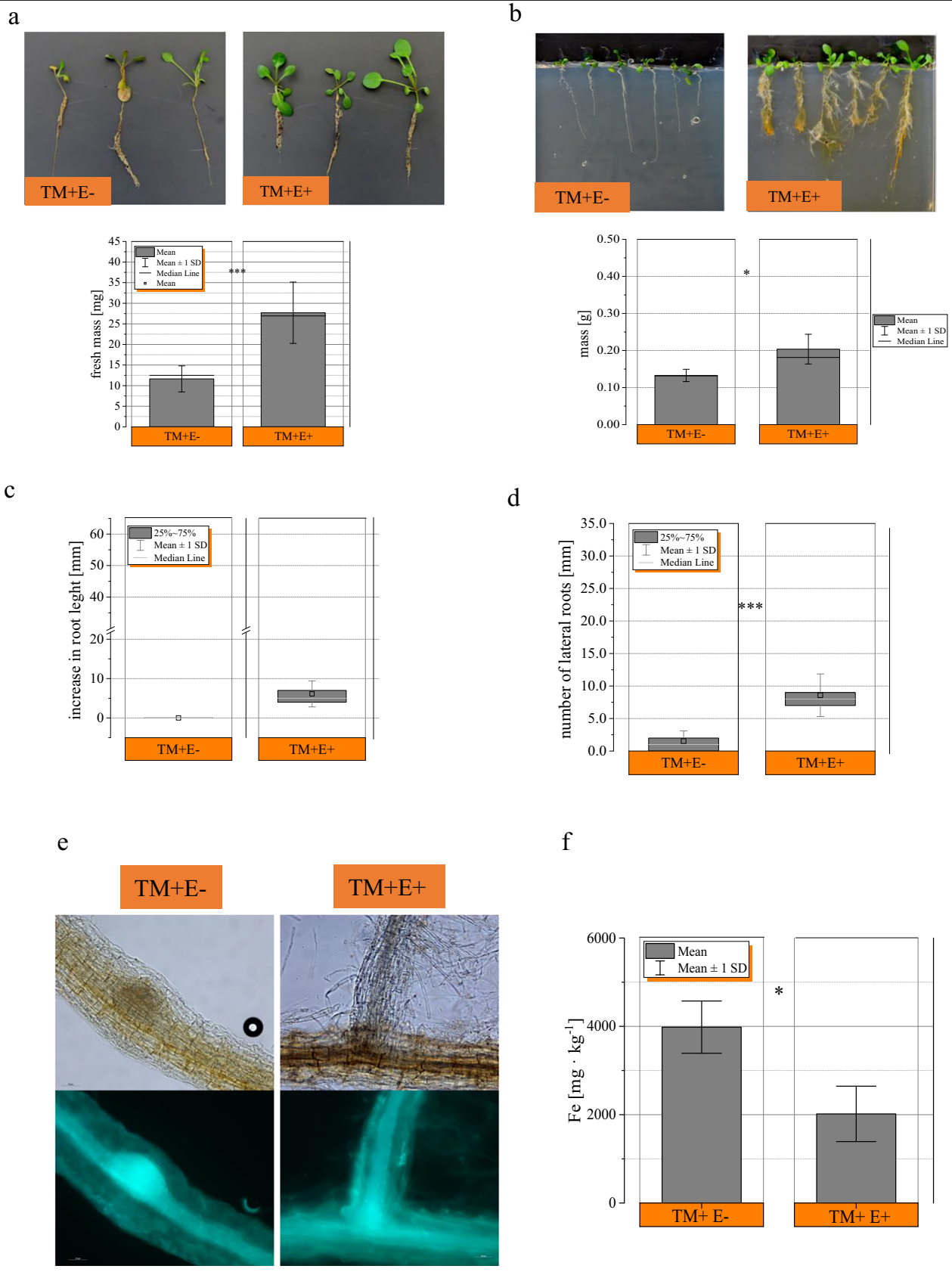
a
TM+E-
TM+E+
fresh mass [mg]
Mean
Mean ± 1 SD
Median Line
Mean
***
b
TM+E-
TM+E+
mass [g]
*
c
increase in root leght [mm]
25%~75%
Mean ± 1 SD
Median Line
d
number of lateral roots [mm]
***
e
TM+E-
TM+E+
f
Fe [mg · kg-1]
*
TM+ E-
TM+ E+

environment. Metal concentrations were experimentally determined to be sublethal for uninoculated plants (E−) *in vitro*. First, the metal precursors in the form of ferric chloride, cadmium sulphate and zinc acetate were dissolved and added to the previously sterilized Strullu and Romand (MSR) medium. The concentrations of metals in mind dump are Zn - 183 mM, Fe – 179.2 mM, and Cd - 890 μM. Determination of the sublethal concentration of metals started from 3 % of the dump soil concentration (Bolesław) and was decreased subsequent to 2.5 ‰ for the TM adapted population (Fig. 2b and Fig. S1). According to the results, which revealed that up to the concentration of 5 ‰, the plants were too stressed, as seen from the condition of the plants, which exhibited poor root development and leaf etiolation, although at the cut-off concentration of 5 ‰, the plants were in the condition that was near the optimum concentration for planned experiments. According to this finding (Fig. 2b), the sublethal concentrations of metals in the medium were 458 μM, 448 μM and 2.22 μM for Fe, Zn and Cd, respectively (Table 1).

2.7. Microscopic observation of roots

After transferring the plants to MSR media (supplemented with metals TM+, control without metals), the root tip was marked on a petri dish, and the plants were inoculated with *S. ruberrimus*. Six days after inoculation, the growth of the main root and the development of lateral roots were evaluated. The root architecture was imaged with an optical scanner and processed with WinRhizo software (Regent Instruments, Que., CA). During this step, root samples were also prepared for microscopic imaging. Microscopic observation was carried out using a Zeiss Axio Imager 2 (Zeiss, DE).

2.8. Determination of metal concentration in plants

A. arenosa samples were washed with 0.1 M Na_2EDTA and ddH_2O (5 samples, 8 plants per sample were prepared) were dried at 80 °C in an oven and quantitatively transferred to a Teflon autoclave with 2 mL of 65 % solution of HNO_3. The suspension was maintained for 1 h at ambient temperature, and then 0.500 mL of 30 % hydrogen peroxide was slowly dropped into the solution and maintained for 0.5 h at ambient temperature. Subsequently, the suspension was mineralized in a microwave digestor for 35 min. The supernatant was quantitatively transferred to a graduated 10 mL volumetric flask and made up with deionized water. To determine the metal concentration, the calibration curve method was used. Fe were analysed using FAAS. The external standard calibration curve was used to quantify the metal concentration. The international standard ERM – CD281 for validation was used (Ważny et al., 2021b).

2.9. Transcriptomic analysis

2.9.1. Transcriptomic analysis of plants

2.9.1.1. RNA isolation. Total RNA was extracted from plant roots and shoots separately with the use of the MagMax™ Plant RNA Isolation Kit (ThermoFisher Scientific, US). For a single sample 10 roots and 10 shoots were pooled. Five samples per treatment (inoculated and not inoculated plants cultured in medium supplemented with toxic metal) were prepared. DNA was digested with DNase I amplification grade (Merck Millipore, US). The analysis of RNA purity and quantity was performed with the use of Nanodrop (ThermoFisher Scientific, US), and the integrity was assessed with the Agilent 2100 Bioanalyzer (Agilent, Santa Clara, CA, US).

2.9.1.2. Preparation of libraries. Whole transcriptome libraries were prepared using the TruSeq Stranded Total RNA LT Sample Prep Kit (Plant) (Illumina, San Diego, CA, US). One thousand nanograms of total RNA (treated with DNAse) was purified from rRNA by rRNA depletion. Subsequently, RNA was purified, fragmented, and primed with random hexamers for first-strand cDNA synthesis and second-strand synthesis. AMPure XP beads (Beckman Coulter, Pasadena, CA, US) were used to separate the ds cDNA from the second strand reaction mix. To prevent blunt 3′ ends from ligating to one another during the adapter ligation reaction, a single 'A' nucleotide was added. A corresponding single 'T' nucleotide on the 3′ end of the adapter provides a complementary overhang for ligating the adapter to the fragment. After this, ligation of indexing adapters to the ends of the ds cDNA was performed, and then PCR with a PCR Primer Cocktail that anneals to the ends of the adapter was performed to amplify the amount of DNA in the library. AMPure XP Beads were used to purify the libraries. The yield and size distribution of the amplified DNA were assessed with an Agilent DNA 1000 Kit using a 2100 Bioanalyzer (Agilent Technologies, USA). Indexed DNA libraries were normalized to 10 nM in the Diluted Claster Template (DCT) plate and then pooled in equal volumes in the Pooled DCT (PDP) plate. Sequencing was performed using the Illumina platform.

2.9.2. Bioinformatics

The RNA-Seq analysis focused on determining types of changes that occur on transcriptomic level in plants inoculated (E+) in comparison to plants uninoculated. To assure best possible quality of analysis the quality control and adapter trimming steps were performed with use of the fastp software (v0.12.4). The fastp is currently the most robust software for data pre-processing. Next, the k-mer based read alignment (pseudoalignment) with mapping and quantification was performed with use of the kallisto (v0.46.2). kallisto allows for ultra-fast gene mapping along with quantification with use of Transcipts-Per-Milion (TPM) normalization. However, the TPM normalization was later on discarded due to use the Trimmed Mean of M-values (TMM) normalization method (included in limma library), which has been more suited to the experiment (Robinson and Oshlack, 2010).

The programming language and ecosystem of choice was the R (v4.0.4) with the Bioconductor ecosystem in (v3.12), with use of BiocManager (v1.30.10).

The preliminary Differential Expression (DE) analysis was performed with DESeq2(v1.30.1), edgeR(v3.32.1) and limma (v.3.46.0). After interpretation and cross-comparison of preliminary findings from DE analysis the analysis with final adjustments was performed with use of limma.

After establishing the key differences between cohorts, the need for further explanation pointed towards Gene Ontology Term Enrichment. The library of choice for that task was topGO (v2.42.0) with GO.db (v3.12.1) and org.At.tair.db (v3.12.0). The topGO allows to perform enrichment analysis with plenty of test statistics and different method to eliminate similarities between GO terms. For current setup the elim algorithm and Fisher statistic were used to prioritize key findings on low level of abstraction – node size set to 1. For demonstrational purposes, on figures show the results of analysis with node size set to 2000, to present our results in an intuitive, graphical form. The results of analyses were interpreted in regards to the findings.

The source code for the RNA-Seq analysis have been uploaded to GitHub repository for open access and reproducibility - https://github.com/bioinf-mcb/bioinf-mcb-rnaseq_arenosa_thaliana_20_22

2.10. Determination of metal concentration in precipitate and culture medium

S. ruberrimus cultured in 2 % malt extract medium for 72 h were centrifuged at 5200 rpm. The precipitate of the fungal culture was washed with deionized water and dried at 105 °C, and the mass was determined. The pellet was then transferred quantitatively to a beaker, and 1 mL of 65 % nitric acid was added. After boiling and cooling to RT, 0.5 mL of 30 % hydrogen peroxide was added, boiled again and kept at this temperature for 30 min. After cooling to RT, the solution was quantitatively transferred to a 5 mL flask and fill up to the mark with deionized water. The iron concentration was determined by means of FAAS compared to the calibration curve.

2.11. Culture medium pH determination

After sterilization and addition of sterile metal solutions (concentrations as above), the liquid medium was cooled to 30 °C, 10 mL of deionized water

was added, and the pH was measured with a pH-metre EC-metre (TRIMETER, CA).

2.12. Perl's staining

Fungus and medium were stained using Perl's method (Brumbarova and Ivanov, 2014). The samples were transferred to the evaporator for 1.5 h and maintained under vacuum (500 mbar) in a fixing solution (methanol: chloroform: glacial acetic acid [6:3:1]). A fresh staining solution, preheated to 37 °C, for colorization was used - 4 % $K_4[Fe(CN)_6]$ and 4 % HCl (v/v). The samples were washed with distilled water and stained for 30 min under vacuum (500 mbar). After staining, the samples were washed 3 times with distilled water (1–2 min each). Microscopic analysis was carried out using a Zeiss Axio Imager 2 (Zeiss, DE).

2.13. X-ray diffraction (XRD)

The obtained precipitates were characterized by X-ray diffraction to identify the exact phase and, according to this, the exact chemical composition. The experiments were carried out using an Xpert'Pro diffractometer (PANalytical, Malvern, UK) equipped with Cu Kα radiation in the range of 5–65° 2θ with a scanning step at 0.02° 2θ.

Mineralogical composition of mine dump soil was also determined using X-ray diffraction (XRD). XRD analyses of powdered samples were performed using a Θ − 2 Θ Rigaku Mini Flex 600 diffractometer. A voltage of 40 kV and 15 mA current were applied. The samples were irradiated by Cu Kα radiation and the data were collected in the range of 2–70° 2Θ, with a step of 0.005°. QUALX2.0 software was used to identify mineral phases (Altomare et al., 2015).

2.14. Scanning electron microscopy - energy dispersive X-ray analysis (SEM-EDX)

The surface morphology of the obtained precipitates (after drying at 105 °C for 12 h) was determined using SEM analysis with a scanning electron microscope (FEI Company Nova Nano SEM 200, Hillsboro, OR, USA) operating in back-scattered electron mode. The distribution of elements was identified by performing SEM/EDS mapping. A JEOL 5400 scanning microscope (JEOL USA, Inc., Peabody, MA, USA) with a LINK ISIS microprobe analyser (Oxford Instruments, Tubney Woods Abingdon, Oxfordshire, UK) was used.

For detailed mineral characteristic of mine dump soil, a field emission scanning electron microscope (FE-SEM, HITACHI S-4700, Japan) with an energy-dispersive spectrometer (EDS, NORAN NSS; Madison, USA) at the Institute of Geological Sciences, Jagiellonian University in Krakow, Poland was employed. Rough preparations were placed on carbon holder and coated with carbon. An accelerating voltage of 20 kV and current of 10 μA were used for imaging and chemical analysis. Backscattered electrons (BSEs) were utilized for imaging. For the chemical analysis in spots, a 100 s acquisition time and the standardless method of quantification were used.

2.15. X-ray photoelectron spectroscopy (XPS)

To analyse the surface composition of the precipitate, X-ray photoelectron spectroscopy (XPS) was used. XPS measurements were carried out using a Prevac photoelectron spectrometer equipped with a VG SCIENTA R3000 hemispherical analyser (Scienta Onicron, Uppsala, Sweden) and a monochromatized aluminium source Al–Kα (E = 1486.6 eV). To compensate for charge accumulation, a low-energy electron flood gun (FS40A-PS) was used. Measurements were performed in high vacuum; hence, the samples were dried at 105 °C before the analysis. For qualitative analysis, specific binding energies were used. The quantitative determination of species was carried out on the basis of the band areas and binding energies of Fe, O, and C. For this purpose, Gaussian–Lorentzian peak shape fitting after a Shirley background correction was applied using CasaXPS software (Casa software Ltd., Teignmouth, UK).

2.16. X-ray fluorescence spectroscopy (XRF)

Elemental screening was performed using an energy dispersive X-ray fluorescence spectrometer (Tracer III SD, Bruker). Analyses were performed using liquid (mineralized) samples placed in cups (Model SC-4340, Fluxana) with bottoms covered with foil (TF-145 Kapton, Fluxana, Tianjin, China). The lamp current was set to 10 μA. Spectra were collected for 120 s.

2.17. UV–Vis spectroscopy

For the determination of the electronic structure of the obtained precipitates, *in situ* UV–Vis spectroscopy analysis was carried out. For this purpose, an AvaSpec-ULS3648 High-resolution spectrometer equipped with an AvaLight-DHc Full-range Compact Light Source (Avantes BV, Apeldoorn, The Netherlands) was used.

2.18. Fourier transform infrared spectroscopy (FTIR)

The consortium (or root in the case of negative control) was taken from the medium using sterile inoculation loop. For the analysis, roots were dried at 80 °C for 12 h and measured directly using the ATR compartment of the FTIR spectrometer. ATR-FTIR analysis was carried out using a Thermo IS10 (Waltham, MA, US) spectrometer equipped with an MCT detector and ATR accessory. The spectra were obtained by averaging 128 scans in the range of 4000–650 cm^{-1} with a 4 cm^{-1} resolution.

2.19. Transmission electron microscopy - selected area electron diffraction (TEM-SAED)

TEM (T20-FEI Technai transmission electron microscopy) imaging was employed to evaluate the morphology, shape and size of the iron based material. The microscope was operated at 200 kV with a LaB6 electron source fitted with a SuperTwin objective lens allowing a point-to-point resolution of 2.4 Å. Selected area electron diffraction (SAED) was performed to elucidate the sample nature (amorphous or crystalline).

2.20. Statistical analysis

Statistical analyses were carried out using Origin 2022 software (OriginLab, Northampton, MA, USA). The results were considered significantly different at $p \leq 0.05$ (*), $p \leq 0.01$ (**), and $p \leq 0.001$ (***). Data normal distribution and variance homogeneity were assessed with Shapiro–Wilk and Levene's tests, respectively. Differences were tested by Student's *t*-test and Tukey's post-hoc one-way analysis of variance (ANOVA) depending on the experimental setup. The detailed descriptions are provided within the results description.

3. Results

3.1. Inoculation with the fungus protects the host against metal toxicity

According to macroscopic observations, *A. arenosa* inoculated with *S. ruberrimus* (E+) exhibited higher TM tolerance than uninoculated plants both in mind dump substrate and *in vitro* MSR medium experiments (Fig. 2a and b - photographs). Biomass production (Fig. 2a and b) was significantly higher in E+ plants; it nearly doubled the biomass of noninoculated *Arabidopsis* (n = 30), Student's *t*-test, (for 2a $p \leq 0.001$ and for 2b $p \leq 0.05$). The roots of plants cocultured *in vitro* with the fungus in TM+-enriched medium were longer than those of noninoculated plants (Fig. 2c and Fig. S2a) {for noninoculated plants, we observed total inhibition of root growth, but inoculation did not completely reverse the effect of metal on root growth, since plants cultured on medium supplemented with metals exhibited root growth inhibition that those cultured on MSR metal-free medium (n = 23, Student's *t*-test, $p \leq 0.001$) (Table S1)}. E+ plants cultured in TM-enriched medium developed a significantly higher number of lateral roots (Fig. 2d) (n = 19, Student's *t*-test, $p \leq 0.001$).

Other root parameters measured, such root surface area and main root total length and the image of scanned roots, are presented in Fig. S2a–c. For both parameters, surface area ($n = 19$, Kruskal–Wallis test, $p \leq 0.001$) and root length ($n = 19$, Kruskal–Wallis test, $p \leq 0.001$), the addition of metals to the medium caused a significant decrease. Considering the metal enrichment conditions, inoculation positively influenced the root surface area (Fig. S2b), and there were no significant changes in the root total length of the main root (Fig. S2c). Microscopic observations clearly showed that the number of lateral root buds in E+ and E− *A. arenosa* cultured in medium supplemented with TM did not differ; however, in E− plants, buds did not develop into lateral roots; most of the buds formed in the pericycle buds did not extend past the cortical layer of the root, most likely due to metal intoxication (Fig. 2e).

Similar results were already shown in Domka et al. (2023). Plant growth was promoted by the fungus independently of the experimental setup; plants were cocultured with *S. ruberrimus* in mine dump substrate, sand and perlite spiked with different metals and in *in vitro* cultures. Due to high metal solubility in the medium, metal concentrations were significantly lower in the medium compared to mine dump concentrations (Table 1). The metal: Zn, Cd and Fe ratios were the same *in vitro* as the metal ratio in the mine dump, except for Fe, whose concentration decreased 10 times due to the solubility and medium optimisation (Table 1). Pb was excluded from the medium due to its low availability in the mine dump substrate. *In planta*, Pb concentrations were quantified as just above the detection limits (Domka et al., 2023). The results of the metal concentration in dump soil show the total amount of elements extracted with aqua regia. It is not possible or reasonable to try preparing medium with the same concentration of metals as in dump. The examination of contaminated soil is quite complicated due to the particular kinetics and equilibrium in the formation of new coordinated individuals by chemical complexation, especially in the presence of organic matter (Ikram et al., 2018).

To analyse the mine dump composition, particularly in terms of bioavailability of metal(oids) analysis of mineralogical composition was performed. X-ray diffraction analysis confirmed that the mine dump soil used for the experiments was composed mostly of quartz (SiO_2), dolomite ($CaMg(CO_3)_2$), calcite ($CaCO_3$), plagioclase ($NaAlSi_3O_8$ – $CaAl_2Si_2O8$) and two types of iron sulphides (FeS_2) – pyrite and marcasite (Fig. S3). Complementarily, SEM-EDS analysis was performed (Suplementary 2 materials – SEM-EDS analysis of all soils) to further characterise the soil and determine metal-containing minerals. To facilitate location of metal bearing, including iron bearing, minerals, the BSE mode was used for imaging. The results of this analysis confirmed that the most common form of Fe occurrence were iron sulphides.

Pb was present mostly in the form of lead carbonates, and much less commonly in mineral form of galena. Zinc minerals were observed in form of zinc sulphides. Low concentration of Zn was additionally detected in multiple minerals. Notable occurrence of Zn, Fe as well as Pb are the admixtures of these elements in carbonates (mostly dolomite). Zn was also determined is some iron sulphides. Traces of iron sulphates were confirmed only by SEM-EDS results (Supplementary 2 materials). Results indicate that iron oxides precipitation is possibly occurring on the very surface and within the porous space of larger, weathering minerals, however the oxygen concentrations, if present in the analytical points were also Fe and S were detected, are very low.

X-ray diffraction analysis of minerals separated from the rhizosphere and bulk soil for both the TM + E+ and the TM + E− experiments (Fig. S4) was performed. The spectra obtained are similar, thus the same minerals presence was determined in slightly different proportion. In both spectra the most prevalent minerals are quartz, dolomite and calcite. Two minerals not detected in the mine dump soil used for the experiments (Fig. S3), were identified as gypsum ($CaSO4{\cdot}2H_2O$) and ankerite ($Ca(Fe, Mg,Mn)(CO_3)_2$). Marcasite and plagioclase were also present in the examined soils.

The phases observed by SEM (Supplementary II – Fig. 2A, B) occur mostly in form of complex aggregates containing metals. The SEM-EDS results align with X-ray diffraction results, and additionally indicate presence of other, including metal-bearing, phases. For both samples those were mostly iron and zinc sulphates as well as sulphides, iron and zinc oxides, and carbonates containing Zn, Fe and Pb (mainly dolomite). Although some differences between TM + E− and TM + E+ rhizosphere-soil mineralogical composition could be observed, taking into account the complexity/heterogeneity of soils, and methodological limitations those are insufficient to draw any conclusions. The visible differences occur between mine dump soil and the TM + E− /TM + E+ rhizosphere-soil samples were the concentration of oxygen in metal bearing phases is higher, and pyrite as well as galena were not detected.

3.2. Plants cocultured with yeast accumulated less Fe than uninoculated plants

A significant decrease in Fe uptake was observed in plants inoculated with the fungus (Fig. 2f). The Fe concentration measured in relation to dry weight decreased twofold from 4000 to 2000 $mg{\cdot}kg^{-1}$ ($n = 3$, Student's *t*-test, $p \leq 0.05$). These results were in line with Domka et al. (2023). In that study we showed that *A. arenosa* and *A. thaliana* inoculated with *S. ruberrimus* accumulated significantly less Fe in both plant shoots and roots. Inoculation had no effect on Zn and Cd accumulation by the plant, therefore, further research focused on plant Fe uptake and metal transformation by the microorganism. Additionally, according to macroscopic observations, in the case of plant–fungus coculture from metal-supplemented medium, the pigmentation of the fungus inhabiting plant roots changed from pink in the control medium to orange, which can be related to changes in fungal dyes, but it must be confirmed and studied in detail (Jędrzejczyk et al., in preparation).

3.3. The transcriptome of plants cocultured with S. ruberrimus shows downregulation of the plant stress response under metal toxicity

The comparison of global gene expression of *A. arenosa* E+ and E− ($n = 5$) cultured in "mine dump" medium revealed significant changes in the transcriptome of *A. arenosa* inoculated with *S. ruberrimus*. After quality control, an average of 43,668,168 reads per sample corresponding to an average of 29,041 unique genes were identified. This corresponded to an average 82 % overall alignment and an 88.45 % gene coverage. According to Limma (corrected p value ≤ 0.05), 5754 genes were differentially expressed in E+ *Arabidopsis vs.* E− roots. The expression of 3048 genes was upregulated in E+ plant roots, whereas the expression of 2706 genes was downregulated (Fig. 3a). In *Arabidopsis* shoots, the expression of 162 and 112 genes was up- and downregulated, respectively (Fig. 3b). The full results of the analysis were deposited at NCBI #SUB11885033. Functional categorization of the differentially expressed genes revealed that the most significantly enriched GO terms (biological process) were related to the plant response to stress/stimulus. This was particularly evident in plant roots, where the top four most highly enriched GO terms accounting for close to 20 % of the overall differentially expressed genes were plant stress response related (GO terms: response to stress, cellular response to stimulus, response to chemical, response to abiotic stimulus). Other notable biological processes altered by the fungus were related to P metabolism (GO term: phosphorus metabolic process) and transport. In plant shoots,

Fig. 3. (Experiment 2). The comparison of global gene expression of plants treated with TM and inoculated with *S. ruberrimus*. Plants were cultured *in vitro* on medium supplemented with Fe(III), Zn(II), Cd(II) (TM+) for 10 days, inoculated (E+) and not inoculated (E−) with *S. ruberrimus* ($n = 5$): a–b) MA plots of transcriptomic data for roots and shoots of E+ and E− *A. arenosa* treat with TM; c–d) the enriched biological processes GO terms searched among differentially expressed genes in roots and shoots of E+ TM-treated *A. arenosa*; e) heatmap representing 2-fold change difference (log2 normalized, adj. p value ≤ 0.05) in the expression of genes involved in stress response (GO terms: response to stress) in roots of TM-treated *A. arenosa* inoculated with the fungus; f) heatmap showing 2-fold change difference (log2 normalized, adj. p value ≤ 0.05) in the expression of genes involved in stress response (GO terms: response to stress) in shoots of E+ *A. arenosa* treated with TM.

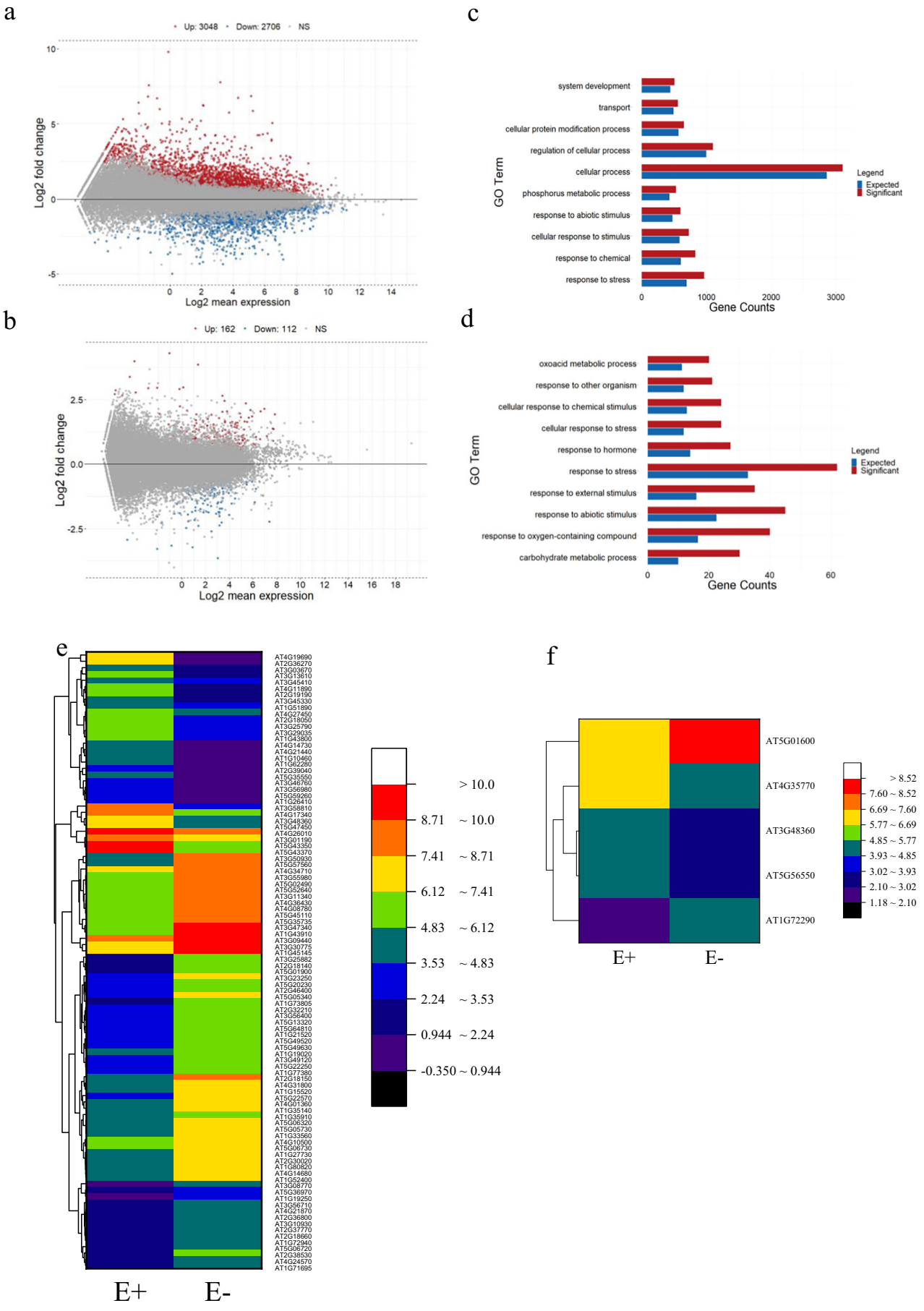
a
Up: 3048
Down: 2706
NS
Log2 fold change
Log2 mean expression
b
Up: 162
Down: 112
NS
Log2 fold change
Log2 mean expression
c
system development
transport
cellular protein modification process
regulation of cellular process
cellular process
phosphorus metabolic process
response to abiotic stimulus
cellular response to stimulus
response to chemical
response to stress
GO Term
Gene Counts
Legend
Expected
Significant
d
oxoacid metabolic process
response to other organism
cellular response to chemical stimulus
cellular response to stress
response to hormone
response to stress
response to external stimulus
response to abiotic stimulus
response to oxygen-containing compound
carbohydrate metabolic process
GO Term
Gene Counts
Legend
Expected
Significant
e
E+
E-
> 10.0
8.71 ~ 10.0
7.41 ~ 8.71
6.12 ~ 7.41
4.83 ~ 6.12
3.53 ~ 4.83
2.24 ~ 3.53
0.944 ~ 2.24
-0.350 ~ 0.944
f
AT5G01600
AT4G35770
AT3G48360
AT5G56550
AT1G72290
E+
E-
> 8.52
7.60 ~ 8.52
6.69 ~ 7.60
5.77 ~ 6.69
4.85 ~ 5.77
3.93 ~ 4.85
3.02 ~ 3.93
2.10 ~ 3.02
1.18 ~ 2.10

the most significantly altered process was the carbohydrate metabolic process. In addition, the symbiotic microorganism significantly affected plant hormone homeostasis (GO term: response to hormone), oxoacid metabolism (GO term: oxoacid metabolic process) and, as stated previously, the plant stress response (GO terms: response to oxygen-containing compounds, response to abiotic stress, response to external stimulus, response to stress and cellular response to stress). Fig. 3c and d represent the top 10 GO terms enriched in E+ *A. arenosa* cultured in mine dump medium. In plant roots, the GO term response to stress was the most significantly ($p = 1.0{\cdot}10^{-30}$) enriched biological process in E+ *A. arenosa*, whereas in plant shoots, its significance was lower ($p = 6.1{\cdot}10^{-5}$). Nevertheless, most genes differentially expressed in the shoots of E+ plants were related to the plant response to stress. In the roots, the expression of 960 genes (adjusted p value ≤ 0.05) related to the stress response was differentially expressed in plants inoculated with *S. ruberrimus*. The expression of the vast majority of the genes (617) was downregulated, whereas the expression of 344 was upregulated (Fig. 3e).

In plant shoots, the expression of a number of differentially expressed genes under metal toxicity in E+ was significantly lower than that in plant roots. Thirty four out of the 62 differentially expressed genes were upregulated, whereas the expression of 28 genes was downregulated (Fig. 3f). For the purpose of presentation, only genes with differential expression of minimum 2-fold up and down were shown in heat maps.

3.4. Metal precipitation by S. ruberrimus

Macroscopic and microscopic observations of plant roots and the gene expression profile of E+ *A. arenosa* suggested that the fungus protected its host by limiting plant exposure to the metals present in the medium. To verify this hypothesis, the ability of the fungus to precipitate metals in the medium was tested. For the simplification of the experimental model, we tested whether the fungus can precipitate metals in liquid medium without the plant. To further verify this, the fungus was cultured in a 2 % water solution of malt extract supplemented with metal ions at the same concentration as in MSR medium (Fig. 4a–b). The viability of the fungus was negatively affected by TM supplementation, but it remained viable as the OD of the culture tended to grow over time (data not shown). To test the ability of the fungus to produce the precipitate, three culture variants were prepared. In the first variant, the concentration of metals (Fe, Zn, Cd) in the culture medium was set at the concentration level of Bol medium used in this study; in the second variant, the medium was supplemented only with Fe (at the same level as in Bol medium), and the third variant was the control sample (malt medium). The fungus was able to produce a black precipitate in medium supplemented with TM in both setups. In cultures (supplemented with Zn and Cd independently) no black precipitate was found (data not shown).

3.4.1. Spectroscopic and diffractometric characterization of precipitate

The precipitate was characterized using spectroscopic and microscopic methods. First, the bulk composition was evaluated using X-ray fluorescence spectroscopy (XRF) (Fig. 4c). Six main elements were identified based on band attribution: Cl (2.62 keV), Ar from the atmosphere (2.95 keV), K (3.31 keV), Fe (K_α = 6.40 keV, K_β = 7.06 keV), Ni (K_α = 7.48 keV, K_β = 8.26 keV), and Zn (K_α = 7.48 keV, K_β = 8.26 keV). In the spectra, bands with energies above 19 keV were also present, which were attributed to the XRF source, and they were no longer considered. Based on qualitative and semiquantitative analyses with XRF, more abundant elements identified by XRF were selected for quantitative analysis by atomic absorption spectrometry (AAS). The analysis showed that the precipitate formed by the fungus contained a significant amount of iron with negligible amounts of zinc and nickel. The concentrations of Fe, Zn and Ni are shown in Fig. 4d. Scanning microscopy imaging with X-ray analysis was performed to determine the morphology of the sediment as well as the elemental distribution. The sediment showed a homogeneous structure, without a defined shape, with inclusions on the surface of larger grains (Fig. 5a–b). The elemental distribution (Fig. 5c) showed the presence of iron in every part of the grain (inclusions and flat surface) at a level of 15 %. The sediment also contained other elements, such as O, P, and N, which are the building blocks of organic matter (remains of fungal cells) and evenly distributed zinc at a level of <1 %. Surface visualization of the distribution of elements (Fig. 5d) revealed that the deposit consisted mainly of iron, which was evenly distributed, and a small amount of zinc, which also showed an even distribution. To determine the oxidation state of elements, it was necessary to perform XPS analysis. The spectrum obtained revealed the presence of C, O, Fe and Zn (Fig. 6a). High-resolution spectra for Fe and Zn were prepared (Fig. 6b and c). After deconvolution, three pairs of bands on the spectra are shown for iron (Fig. 6b): 711.54 and 723.94, 712.43 and 725.90, 717.44 and 728.87 keV. All the bands can be assigned to Fe(II) and Fe(III) species in different chemical environments (compounds) (Novotny et al., 2013; Peng et al., 2022). On the other hand, one pair of bands for Zn was found: 1022.00 and 1045.47. The bands can be assigned to zinc oxide (Biesinger et al., 2010; Xu et al., 2013). The next step in identifying the deposit was to carry out X-ray diffraction (XRD) measurements. It is well known that crystalline forms of chemical individuals can be identified using XRD. The results obtained revealed no characteristic reflections for iron or zinc oxides or hydroxides (Fig. S6). Only a broadened band at approximately 20° corresponding to the amorphous phase of iron-mediated compounds was observed (Fu et al., 2016). As a complementary analysis, UV–Vis scanning in reflective mode was performed. No characteristic bands for iron oxide NPs were observed (data not shown). The far-infrared analyses and Raman spectroscopy did not reveal bands characteristic of iron oxides (data not shown) because they were overlapped by the bands assigned for resins of organic matter, as it is not possible to separate the precipitate from the fungal cells.

Visualization by TEM revealed that nanoparticles are not present in the precipitate. No structures with visible dimensions lower than 500 nm were observed. The precipitate seemed to be rather an aggregate than a product of fragmentation of larger particles. Moreover, it was found in both aqueous and organic solvents. According to the SAED patterns, the particles were amorphous since only diffuse rings were observed, indicating that the nanocrystals lacked long range crystalline ordering (Fig. S7).

All of the abovementioned analyses were performed for the precipitate created by the fungus in liquid medium.

3.4.2. The plant-fungus consortium affects Fe speciation in culture

To determine structural changes and metal speciation in culture, we carried out FTIR analysis for roots of the plant–fungus consortium in MSR cultures supplemented with metals (Fig. 7). This analysis was performed for determining the vibrations of specific functional groups. The analysis was based on attribution tables and literature in which similar systems have been studied. On this basis, the relevant functional groups were assigned and those that were affected by the fungus were selected. The spectra revealed bands at 3300 cm^{-1} originating from the vibrations of the —OH groups from proteins, and the water content increased the background line in this region. In the spectra, bands were also present at 2920 cm^{-1} and 2850 cm^{-1}, which were attributed to the stretching vibrations of the —CH groups, symmetric and asymmetric, respectively. Other bands observed were 1740 cm^{-1} and 1245 cm^{-1}, which were attributed to carboxylic acids (C═O stretching) and (C—O stretching), respectively (Bekiaris et al., 2016). The bicarbonate band appeared at 1630 cm^{-1} (Jędrzejczyk et al., 2016). These bands can be assigned to the C═O stretch in proteins and amides type I (Moreno-García et al., 2021). Some phosphorous-associated bands could be recognized in the spectra. First, the calcium phosphate band at 1540 cm^{-1}, then iron phosphate pair bands – main at 1034 cm^{-1} and the satellite at 540 cm^{-1} (Bekiaris et al., 2016). The peaks from 1030 to 1050 cm^{-1} can also be assigned to carbonyl groups (O—C—O) associated with the presence of lipids and carbohydrates (Moreno-García et al., 2021). The main interesting region where the changes were observed is 1600–1100 cm^{-1}. Three bands were observed at 1417, 1370 and 1360 cm^{-1}. The bands can be attributed to vibrations of —CH_2 groups allocated with metals, —CH_2 wagging vibrations in lipids,

a

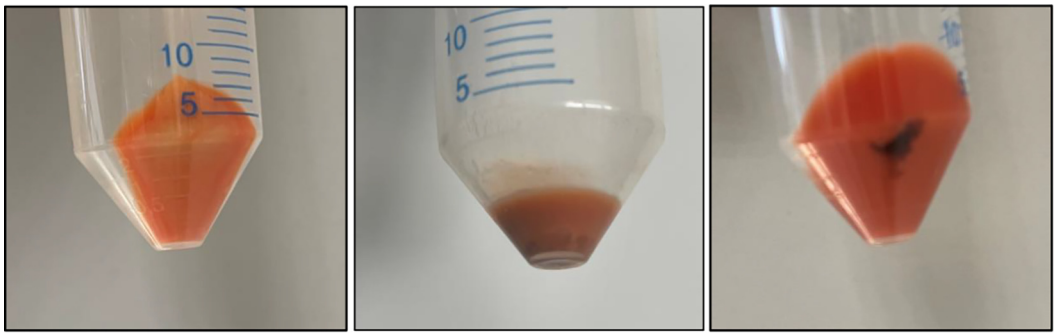

b

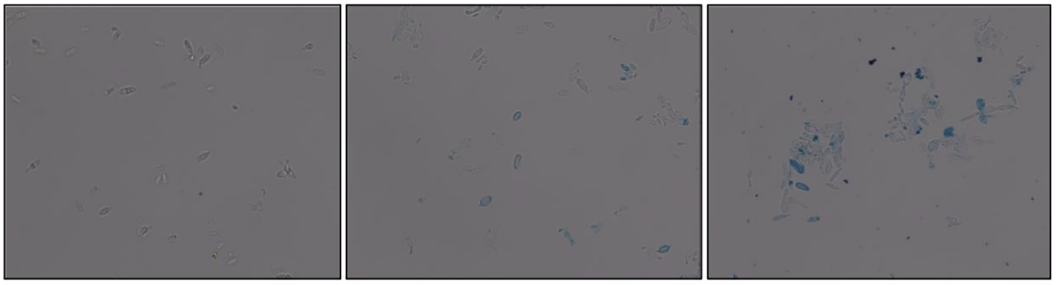

c

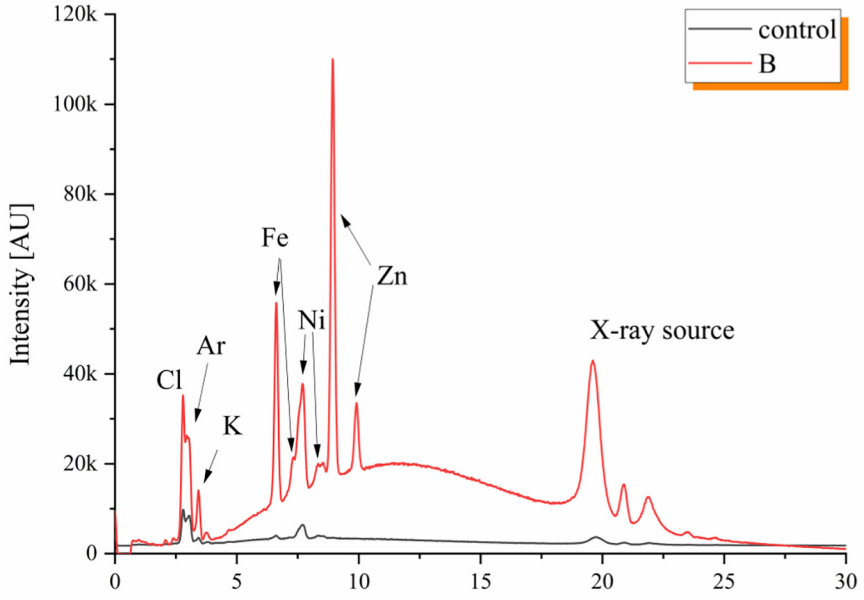

d

Element	Concentration by AAS
Fe	25 [%]
Zn	2000 [mg · kg^{-1}]
Ni	1000 [mg · kg^{-1}]

Fig. 4. (Experiment 3). a) Photographs of centrifuged *S. ruberimus* cultures from medium (from left) control (TM-), supplemented with Fe at TM+ concentration, supplemented with metals TM+ (n = 3); b) microscopic images of *S. ruberrimus* [variannts as in a], XRF spectra of precipitate made by *S. ruberrimus* in TM+ medium, d) AAS results of metals presented in precipitate made by *S. ruberrimus* in TM+ medium (n = 5).

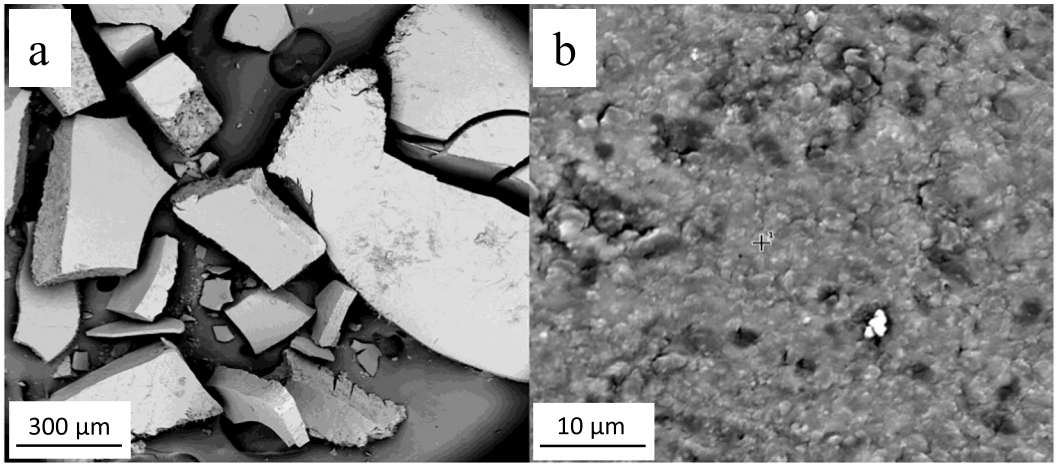

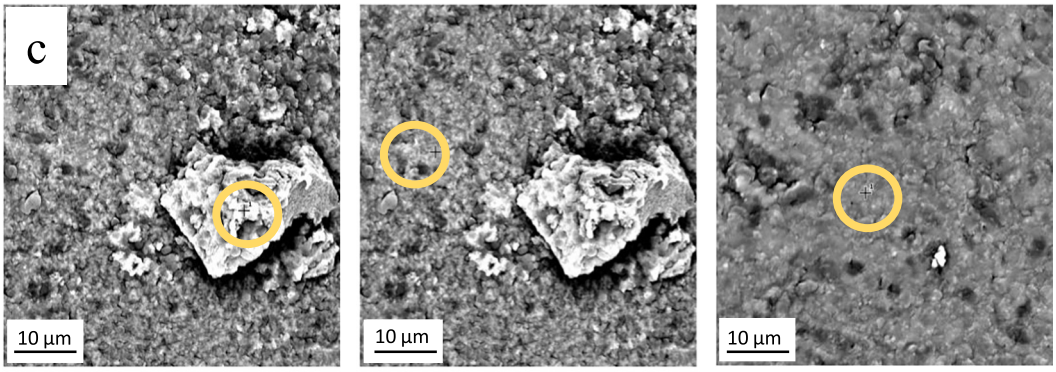

Element Symbol	Atomic Conc.	Weight Conc.
Fe	**19.6**	**43.9**
O	39.7	25.6
P	13.9	17.4
N	2.8	1.60

Element Symbol	Atomic Conc.	Weight Conc.
Fe	**15.13**	**38.5**
O	24.80	18.1
P	9.22	13.0
N	10.16	6.48
Zn	0.74	2.19

Element Symbol	Atomic Conc.	Weight Conc.
Fe	**14.60**	**38.4**
O	20.54	15.5
P	9.14	13.3
N	13.35	8.81

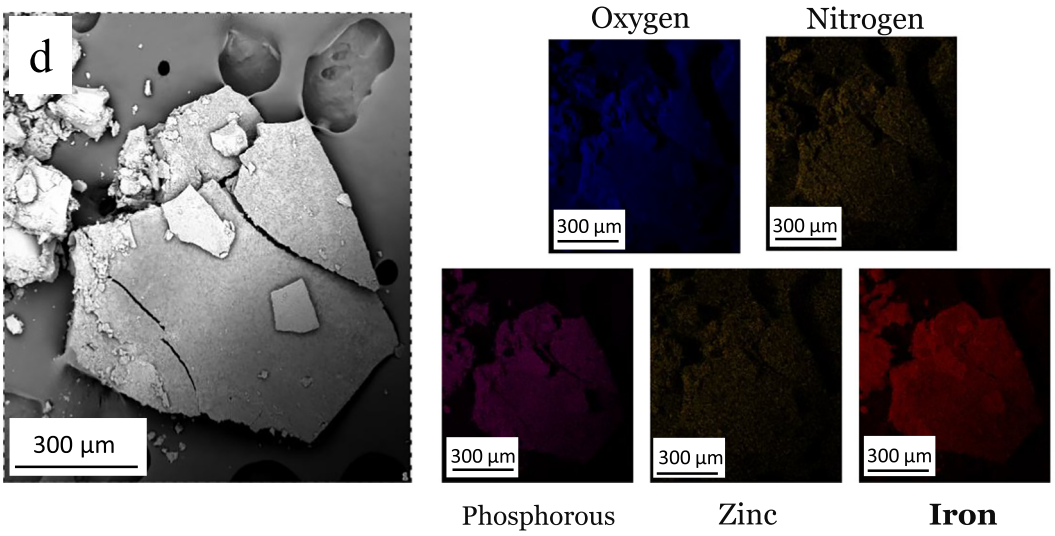

Fig. 5. (Experiment 3). SEM-EDX analysis a–b) precipitate images with different magnifications (n = 3), c) precipitate images with indicated measurement points and corresponding results of elemental analysis, d) EDX elemental mapping of precipitate. The spot area of elemental analysis is ap. 50–70 nm.

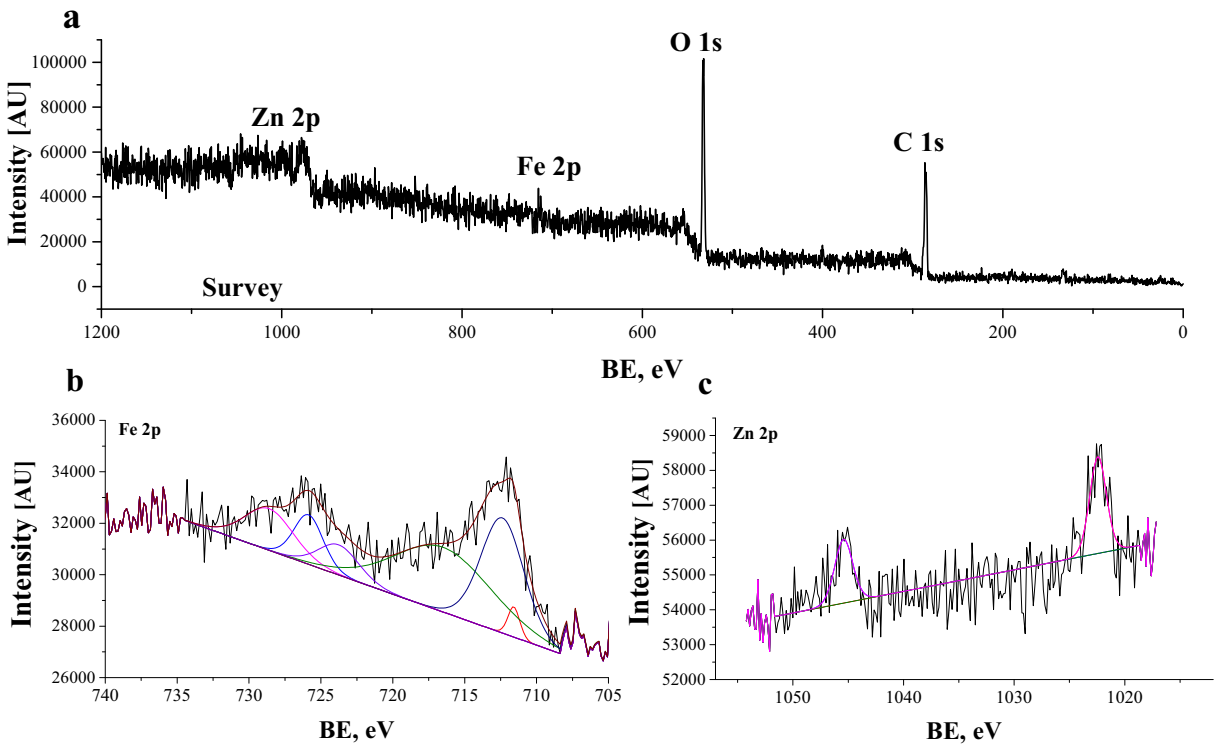

Fig. 6. (Experiment 3). XPS spectra of the precipitate (n = 3), a) overview, b) high-resolution spectrum for Fe, c) high-resolution spectrum for Zn.

and β1,3 glucans, and —CH_2 wagging vibrations in lipids. For the control (TM − E −) variant, one band at 1370 cm^{-1} was observed, which degenerated into two bands at 1417 and 1370 cm^{-1} for plants cultured in the medium with metals (TM + E −). This region is usually attributed to vibrations of organic compounds (functional groups from these compounds, to be more precise), interacting with Fe derivates (Stumm and Blber, 1994). Inoculation reverses the changes in the IR spectrum; in the *A. arenosa – S. ruberrimus* (TM + E +) system bands from the analysed region resemble those observed in plants cultured in medium not supplemented with metals (no band at 1417 cm^{-1}), suggesting stress protection and lower exposition to metal toxicity of plants cocultured with the fungus (TM + E +).

4. Discussion

The complex interplay between the biotic and abiotic elements of the environment determines ecosystem functioning. In environments enriched with toxic metals, pioneer plants and adapted microorganisms were shown to provide the ecosystem with functions necessary for the development of a diverse environment (Flores-Torres et al., 2021; Zhang et al., 2001). In this study, we show that *S. ruberrimus* associated with *Arabidopsis arenosa* could facilitate plant adaptation to metal toxicity by alleviating plant stress. This endophytic fungus was also capable of precipitating excess Fe in medium and likely immobilizing it, making it unavailable to the plant and thus lowering plant exposure to metal toxicity. One route of plant metal uptake

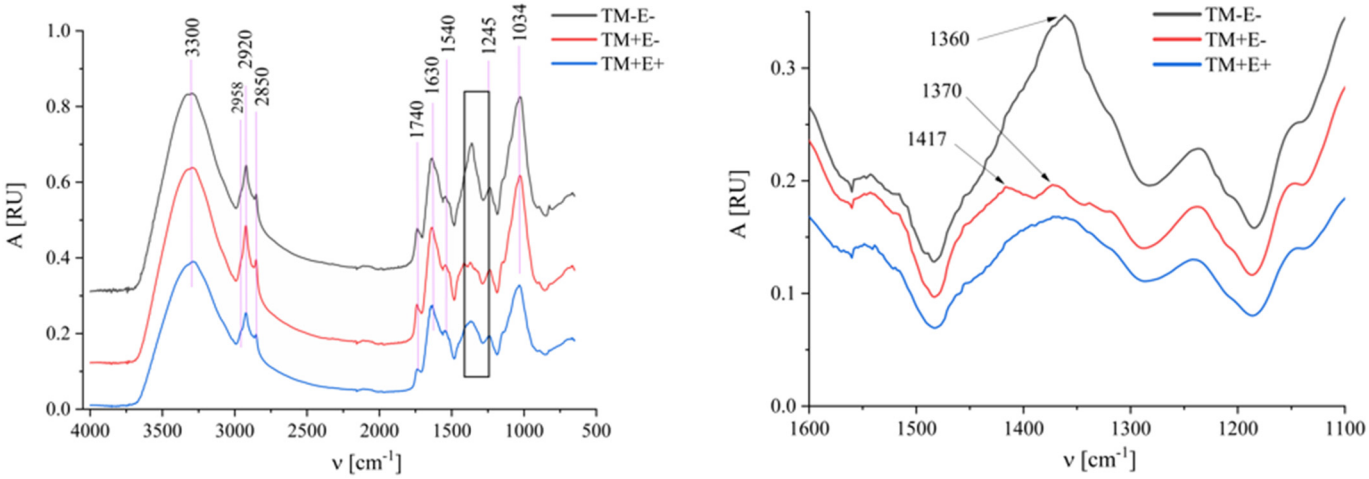

Fig. 7. (Experiment 2). FTIR spectra of *A. arenosa* roots inoculated with *S. ruberrimus* (n = 3), variants TM − E − (negative control): roots of *A. arenosa* cultured *in vitro* in medium without toxic metals and fungus, TM + E − : roots of *A. arenosa* cultured *in vitro* in medium with toxic metals and without fungus, TM + E + : roots of *A. arenosa* cultured *in vitro* in medium with toxic metals and fungus.

inhibition was most likely related to decreased Fe availability in the rhizosphere. Previous studies have shown that symbiotic microorganisms can affect metal uptake by plants (Domka et al., 2019). Not much is known about how this is achieved.

4.1. Analysis of the plants transcriptome provided clues indicating decreased exposition to Fe toxicity of plants inoculated with S. ruberrimus

The majority of the stress-related genes altered in E+ *Arabidopsis* were downregulated, a large proportion were related to defence against biotic (100) and abiotic stress (65). It is worth noting that this group included genes encoding antioxidant enzymes such as proteins from the peroxidase superfamily, catalase 1 (AT1G20630), catalase 3 (AT1G20620) and thioredoxin 5 (AT1G45145). Attenuation of the plant's defence response observed at the level of gene expression together with the root development under metal toxicity, plant biomass yield and the fact that plants took up significantly less Fe suggested that the exposition of E+ plants to toxic metals was lower than that of E− *Arabidopsis* roots. In the mentioned before study (Domka et al., 2023) metal uptake inhibition resulted from alterations in ethylene dependent plant metal uptake mechanisms. Here we show that aside from optimizing plant metal uptake, the symbiotic microorganism may also decrease the exposition of plant roots to toxic metals by decreasing the bioavailability of Fe in medium.

At least some of the alterations in the plant stress response can be also explained by the adaptation of the plant immunological landscape to the interaction with the fungus. According to previous reports, the plant defence system undergoes significant rearrangements during symbiosis (Camehl et al., 2010; Vadassery et al., 2009; Vahabi et al., 2015). In the data shown in this report, the expression of a significant number of genes (close to 40) involved in plant defence against fungi and bacteria was upregulated. Additionally, a large number of genes with upregulated expression were related to ROS homeostasis, such as genes encoding proteins from the peroxidase superfamily (17) and the chalcone and stilbene synthase family protein TT4 (AT5G13930) (Saslowsky et al., 2000; Tropf et al., 1994, 1995). ROS play an important role in plant-microorganism interactions. Their production has been shown to be activated during plant-microorganism interactions, including mutualistic interactions (Scott et al., 2007; Tanaka et al., 2006). Another important aspect of plant metabolism (biological process in transcriptomic analysis) affected by the endophytic yeast was plant carbohydrate metabolism. This has also been reported on several occasions; plants cocultured with microorganisms were shown to exhibit more efficient photosynthesis and altered, possibly optimized carbohydrate allocation (Doidy et al., 2012; Opitz et al., 2021; Rozpądek et al., 2019). We can also assume that plant nutrition was positively affected in symbiotic plants (upregulation of P and N homeostasis genes), which has been previously observed in plants cocultured with beneficial microorganisms (Rozpądek et al., 2019). This indeed indicated optimized plant performance but could not provide a direct link between the inhibition of Fe uptake and plant inoculation with *S. ruberrimus*.

4.2. The fungus was capable of precipitating Fe in in vitro cultures

Yeast cultured in medium mimicking mine dump was able to precipitate Fe in an insoluble form. It is well known that a metal-enriched environment can affect fungal behaviour. The response to this stress can manifest as different structural/chemical changes in the fungal cell or entire fungus–plant consortium. In regard to structural changes, microorganisms can biosynthesize NPs or MPs. This happens especially when the ions are readily available in the substrate (especially in the case when the precursors of metal are highly soluble, ex. nitrates, citrates, *etc.*). The synthesis of nanoparticles by microorganisms has been widely investigated. There are many ways to stimulate microorganisms to produce nanoparticles, including direct contact with metal precursors (Fayaz et al., 2010), irradiation (Saifuddin et al., 2009) and plant extracts (Saifuddin et al., 2009). Microorganisms can synthesize many types of nanoparticles with distinct characteristics, such as biocidal Ag, Au/Ag nanoparticles, nanoparticles of transition metals/oxides such as Fe (Vainshtein et al., 2014), Pd (Chen et al., 2013), ZnO (Jayaseelan et al., 2012) and other metals, oxides and sulphides (reviewed in (Zielonka and Klimek-Ochab, 2017)). In this case, the fungus was able to precipitate a deposit consisting mainly of iron oxides or hydroxides on which zinc and nickel ions were adsorbed. AAS analysis indicated that the precipitate consists mainly of iron, which was confirmed by surface EDX analysis. At the same time, the distribution of iron was uniform and occurred uniformly in the whole sample, whereas the distribution of zinc was homogeneous but restricted only to evenly adsorbed ions within the precipitate. This indicated the inclusion of ions of other metals in the precipitate. Such reports are known from the literature and concern iron plaque on which nutrients and other metals can be adsorbed (Zhang et al., 2019). Both AAS and EDX analysis indicated that the abundance of zinc and nickel within the deposit was significantly lower than that of Fe. EDX mapping also revealed that phosphorus and nitrogen were evenly distributed in the sample, which indicated the presence of residual organic matter in the formed deposit. Therefore, the uptake of toxic metals by plants (if associated with fungi) could be positively influenced. In addition, microscopic analyses indicated iron uptake by the fungus itself. Such an ability of the yeast is known from the literature (Zinicovscaia et al., 2020). This means that the fungus not only precipitated iron in the form of unbound compounds with reduced solubility but also inactivated it on/in the cells. This was mainly due to the physical trapping of metals in a form unavailable to the plant (Chen et al., 2020; Eid et al., 2020). The FTIR confirmed plant stress protection and probably decreased metal exposition of plants cocultured with the endophytic yeast. The mechanism of this inactivation, however, requires further research and goes beyond the purpose of this paper. It needs to be emphasized that we were not able to identify Fe residues in the rhizosphere. This was largely due to difficulties in sample preparation; thus, we can only assume that the fungus is capable of precipitating Fe in coculture with the plant. Nevertheless, the SEM analysis of bulk soil and rhizosphere revealed subtle differences between them. The most prominent difference was the absence of pyrite in rhizosphere (which is observed in bulk soil). This, however, cannot be treated as proof that the fungus transforms pyrite into other Fe individuals, since there is no evidence of pyrite presence in rhizosphere even in the case of plants not inoculated with the fungus. Such findings can be associated with Fe transformation in rhizosphere or, the complexity of system precluded observation of Fe individuals in soil due to its amorphous character or size of those.

Characterization of the precipitate by microscopic and diffractometric methods confirmed that the precipitate consists mainly of iron structures on which zinc ions are adsorbed. Although XRD analysis did not reveal crystalline forms of iron, similar results for the oxides and hydroxides present in the iron plaque were obtained by Fu et al. (2016). For the several types of iron compounds studied, they obtained the same amorphous XRD profiles as in our case. The lack of typical reflections for crystalline iron compounds could be explained by the formation of highly dispersed iron nanoparticles, but these were not visualized either by SEM or shown by UV–Vis, where no typical plasmons for this type of grouping are present. Therefore TEM-SAED analysis was carried out. The results confirmed that no nanosized structures were formed. The precipitate had an amorphous character which confirms the results obtained by SEM, XRD and UV–Vis analyses. Surface analysis with ESCA revealed, in addition to the element characteristics of organic matter, iron and zinc in the deposit. Importantly, up to three types of iron in the second and third oxidation stages were identified, suggesting a mixed nature of the precipitate rather than a single compound. Furthermore, the coexistence of both oxidation states may be an indication of redox equilibrium being established in the system, for which the fungus may be responsible. It is interesting to note the observed high surface concentration of zinc, again with a low concentration in the bulk. Considering that the XPS analysis is typically a surface analysis, this indicates that the zinc actually has adsorbed to the surface of the formed iron precipitate and is thus also being inactivated. This finding is indeed consistent with the uptake of these two metals by the plant inoculated with *S. ruberrimus*.

All analyses carried out indicate that the fungus possesses the ability to precipitate iron in the form of an amorphous mixed precipitate on which

zinc ions adsorb. This likely affects the plant, which takes up less metals and, according to the response at the level of gene expression, experiences less metal stress. It needs to be emphasized though, that we were not able to identify Fe residues in the rhizosphere. This was largely due to difficulties in sample preparation; thus, we can only assume that the fungus is capable of precipitating Fe in coculture with the plant.

5. Conclusion

In this study, an important function of the fungus *Sporobolomyces ruberrimus* was described. It reduces the deleterious effects of increased concentrations of metals in soil/substrate, in this case excess of Fe, on plant functioning. Such an impact can be realized by fine-tuning plant metal homeostasis as well as inactivating metals in the form of precipitates (possibly coordination/adsorption individuals), indicating that the mechanism of Fe uptake inhibition is cumulative rather than unifactorial. Research shows that the plant in the presence of the fungus reacts to the substrate with metals, as if there were significantly fewer metals in it. The precipitate was characterized using microscopic and spectroscopic methods. The results revealed that *S. ruberrimus* can inactive iron by precipitation in the form of mixed oxides, hydroxides or phosphates in amorphous form. The precipitate is similar to iron plaque widely observed in the case of wetland plants such as rice but exhibits a more complex composition – especially that kinetics and equilibrium in soil is quite complicated in comparison to liquid medium. However, we observed the adsorption of Zn ions on the surface of the deposit, which is common for iron plaque, where adsorbed ions (nutrients) are available for plants. Hence, in the case of elevated concentrations of metals other than Fe, they can be adsorbed on Fe deposits and inactivated in this way.

CRediT authorship contribution statement

Roman J. Jędrzejczyk: Conceptualization, Methodology, Validation, Formal analysis, Methodology, Resources, Data curation, Writing – original draft, Writing – review & editing, Visualization, Supervision, Project administration. **Maciej Gustab:** Investigation, Methodology, Writing – review & editing. **Rafał Ważny:** Investigation, Methodology, Writing – review & editing. **Agnieszka Domka:** Investigation, Methodology, Writing – review & editing. **Przemysław J. Jodłowski:** Investigation, Methodology, Writing – review & editing. **Maciej Sitarz:** Investigation, Methodology, Writing – review & editing. **Patryk Bezkosty:** Investigation, Methodology, Writing – review & editing. **Michał Kowalski:** Data curation, Methodology, Writing – review & editing. **Dominika Pawcenis:** Investigation, Methodology, Writing – review & editing. **Kinga Jarosz:** Investigation, Methodology, Writing – review & editing. **Victor Sebastian:** Investigation, Methodology, Writing – review & editing. **Paweł P. Łabaj:** Formal analysis, Writing – review & editing. **Piotr Rozpądek:** Funding acquisition, Conceptualization, Writing – original draft, Writing – review & editing.

Data availability

Data will be made available on request.

Declaration of competing interest

The authors declare that they have no known competing financial interests or personal relationships that could have appeared to influence the work reported in this paper.

Acknowledgements

The authors would like to thank the National Science Centre for funding the research under grants No. 2017/27/B/NZ8/01199 and 2019/33/B/NZ9/01372. The authors would also like to thank Monika Hanula, Magdalena Zyzik and Oliwia Śmieszek for technical support. The authors would like to thank Marcus Puschenreiter for valuable comments on the topic of this research and Piotr Jeleń for help with Raman and far-IR analyses. The open-access publication of this article was funded by the Priority Research Area BioS under the programme 'Excellence Initiative—Research University' at the Jagiellonian University in Kraków.

Appendix A. Supplementary data

Supplementary data to this article can be found online at https://doi.org/10.1016/j.scitotenv.2023.161887.

References

Altomare, A., Corriero, N., Cuocci, C., Falcicchio, A., Moliterni, A., Rizzi, R., 2015. QUALX2.0: a qualitative phase analysis software using the freely available database POW_COD. J. Appl. Crystallogr. 48, 598–603.

Azmat, M.A., Khan, I.A., Cheema, H.M.N., Rajwana, I.A., Khan, A.S., Khan, A.A., 2012. Extraction of DNA suitable for PCR applications from mature leaves of Mangifera indica L. J. Zhejiang Univ. Sci. B 13, 239–243. https://doi.org/10.1631/jzus.B1100194.

Bekiaris, G., Peltre, C., Jensen, L.S., Bruun, S., 2016. Using FTIR-photoacoustic spectroscopy for phosphorus speciation analysis of biochars. Spectrochim. Acta A Mol. Biomol. Spectrosc. 168, 29–36. https://doi.org/10.1016/j.saa.2016.05.049.

Biesinger, M.C., Lau, L.W.M., Gerson, A.R., Smart, R.S.C., 2010. Resolving surface chemical states in XPS analysis of first row transition metals, oxides and hydroxides: Sc, Ti, V, Cu and Zn. Appl. Surf. Sci. 257, 887–898. https://doi.org/10.1016/j.apsusc.2010.07.086.

Bilal, S., Shahzad, R., Khan, A.L., Al-Harrassi, A., Kim, C.K., Lee, I.J., 2019. Phytohormones enabled endophytic Penicillium funiculosum LHL06 protects Glycine max L. from synergistic toxicity of heavy metals by hormonal and stress-responsive proteins modulation. J. Hazard. Mater. 379, 120824. https://doi.org/10.1016/j.jhazmat.2019.120824.

Blute, N.K., Brabander, D.J., Hemond, H.F., Sutton, S.R., Newville, M.G., Rivers, M.L., 2004. Arsenic sequestration by ferric iron plaque on cattail roots. Environ. Sci. Technol. 38, 6074–6077. https://doi.org/10.1021/es049448g.

Brumbarova, T., Ivanov, R., 2014. Perls staining for histochemical detection of iron in plant samples. Bio-Protocol 4. https://doi.org/10.21769/BioProtoc.1245.

Camehl, I., Sherameti, I., Venus, Y., Bethke, G., Varma, A., Lee, J., Oelmüller, R., 2010. Ethylene signalling and ethylene-targeted transcription factors are required to balance beneficial and nonbeneficial traits in the symbiosis between the endophytic fungus Piriformospora indica and Arabidopsis thaliana. New Phytol. 185, 1062–1073. https://doi.org/10.1111/j.1469-8137.2009.03149.x.

Chen, H., Sun, D., Jiang, X., Jing, X., Lu, F., Odoom-Wubah, T., Zheng, Y., Huang, J., Li, Q., 2013. Fabrication of Au/Pd alloy nanoparticle/Pichia pastoris composites: a microorganism-mediated approach. RSC Adv. 3, 15389–15395. https://doi.org/10.1039/c3ra41215f.

Chen, J., Li, N., Han, S., Sun, Y., Wang, L., Qu, Z., Dai, M., Zhao, G., 2020. Characterization and bioremediation potential of nickel-resistant endophytic bacteria isolated from the wetland plant Tamarix chinensis. FEMS Microbiol. Lett. 367, 1–7. https://doi.org/10.1093/femsle/fnaa098.

Clemens, S., 2001. Molecular mechanisms of plant metal tolerance and homeostasis. Planta 212, 475–486. https://doi.org/10.1007/s004250000458.

Coon, M. (Ed.), 1980. Microsomes, Drug Oxidations, And Chemical Carcinogenesis. Vol. 1. Academic Press.

Crowder, A.A., Macfie, S.M., 1986. Seasonal deposition of ferric hydroxide plaque on roots of wetland plants. Can. J. Bot. 64, 2120–2124. https://doi.org/10.1139/b86-279.

Doidy, J., Grace, E., Kühn, C., Simon-Plas, F., Casieri, L., Wipf, D., 2012. Sugar transporters in plants and in their interactions with fungi. Trends Plant Sci. 17, 413–422. https://doi.org/10.1016/j.tplants.2012.03.009.

Domka, A., Jędrzejczyk, R.J., Ważny, R., Gustab, M., Kowalski, M., Nosek, M., Bizan, J., Puschenreiter, M., Vaculik, M., Kovac, J., Rozpądek, P., 2023. Endophytic yeast protect plants against metal toxicity by inhibiting plant metal uptake through an ethylene dependent mechanism. Plant Cell Environ. 46, 268–287. https://doi.org/10.1111/pce.14473.

Domka, A., Rozpądek, P., Ważny, R., Turnau, K., 2019. Mucor sp.—an endophyte of Brassicaceae capable of surviving in toxic metal-rich sites. J. Basic Microbiol. 59, 24–37. https://doi.org/10.1002/jobm.201800406.

Eid, A.M., Fouda, A., Niedbała, G., Hassan, S.E.D., Salem, S.S., Abdo, A.M., Hetta, H.F., Shaheen, T.I., 2020. Endophytic Streptomyces laurentii mediated green synthesis of Ag-NPs with antibacterial and anticancer properties for developing functional textile fabric properties. Antibiotics 9, 1–18. https://doi.org/10.3390/antibiotics9100641.

Emerson, D., Weiss, J.V., Megonigal, J.P., 1999. Iron-oxidizing bacteria are associated with ferric hydroxide precipitates (Fe-plaque) on the roots of wetland plants. Appl. Environ. Microbiol. 65, 2758–2761.

Fayaz, A.M., Balaji, K., Girilal, M., Yadav, R., Kalaichelvan, P.T., Venketesan, R., 2010. Biogenic synthesis of silver nanoparticles and their synergistic effect with antibiotics: a study against gram-positive and gram-negative bacteria. Nanomed. Nanotechnol. Biol. Med. 6, 103–109. https://doi.org/10.1016/j.nano.2009.04.006.

Flores-Torres, G., Solis-Hernández, A.P., Vela-Correa, G., Rodríguez-Tovar, A.V., Cano-Flores, O., Castellanos-Moguel, J., Pérez, N.O., Chimal-Hernández, A., Moreno-Espíndola, I.P., Salas-Luévano, M.Á., Chávez-Vergara, B.M., Rivera-Becerril, F., 2021. Pioneer plant species and fungal root endophytes in metal-polluted tailings deposited near human populations and agricultural areas in Northern Mexico. Environ. Sci. Pollut. Res. 28, 55072–55088. https://doi.org/10.1007/s11356-021-14716-6.

Fu, Y.Q., Yang, X.J., Ye, Z.H., Shen, H., 2016. Identification, separation and component analysis of reddish brown and non-reddish brown iron plaque on rice (Oryza sativa) root surface. Plant Soil 402, 277–290. https://doi.org/10.1007/s11104-016-2802-8.

Gao, X.P., Yao, S.M., Yan, T.Y., Zhou, Z., 2009. Alkaline rechargeable Ni/Co batteries: cobalt hydroxides as negative electrode materials. Energy Environ. Sci. 2, 502–505. https://doi.org/10.1039/b901934k.

Gardes, M., Bruns, T.D., 1993. Gardes and Burns, 1993. Mol. Ecol. https://doi.org/10.1111/j.1365-294X.1993.tb00005.x.

Ikram, M., Ali, N., Jan, G., Jan, F.G., Rahman, I.U., Iqbal, A., Hamayun, M., 2018. IAA producing fungal endophyte Penicillium roqueforti Thom., enhances stress tolerance and nutrients uptake in wheat plants grown on heavy metal contaminated soils. PLoS One 13, 1–22. https://doi.org/10.1371/journal.pone.0208150.

Jayaseelan, C., Rahuman, A.A., Kirthi, A.V., Marimuthu, S., Santhoshkumar, T., Bagavan, A., Gaurav, K., Karthik, L., Rao, K.V.B., 2012. Novel microbial route to synthesize ZnO nanoparticles using Aeromonas hydrophila and their activity against pathogenic bacteria and fungi. Spectrochim. Acta A Mol. Biomol. Spectrosc. 90, 78–84. https://doi.org/10.1016/j.saa.2012.01.006.

Jędrzejczyk, R.J., Chlebda, D., Chrzan, M., Piwowarczyk, E., Sitarz, M., Łojewska, J., Jodłowski, P.J., Kołodziej, A., Węgrzynowicz, A., 2016. In situ and operando spectroscopic studies of sonically aided catalysts for biogas exhaust abatement. J. Mol. Struct. 1126, 132–140. https://doi.org/10.1016/j.molstruc.2016.02.039.

Jing, H., Liu, W., Zhao, Z., Zhang, J., Zhu, C., Shi, Y., Wang, D., Li, Y., 2021. Electronics and coordination engineering of atomic cobalt trapped by oxygen-driven defects for efficient cathode in solar cells. Nano Energy 89, 106365. https://doi.org/10.1016/j.nanoen.2021.106365.

Khan, N., Seshadri, B., Bolan, N., Saint, C.P., Kirkham, M.B., Chowdhury, S., Yamaguchi, N., Lee, D.Y., Li, G., Kunhikrishnan, A., Qi, F., Karunanithi, R., Qiu, R., Zhu, Y.G., Syu, C.H., 2016. Root iron plaque on wetland plants as a dynamic pool of nutrients and contaminants. Adv. Agron. 138, 1–96. https://doi.org/10.1016/bs.agron.2016.04.002.

Kumar, R., Johnson, K.M., Williams, N.X., Subramanian, V., 2019. Scaling printable Zn–Ag 2 O batteries for integrated electronics. Adv. Energy Mater. 9, 1–9. https://doi.org/10.1002/aenm.201803645.

Li, X., Ma, L., Li, Y., Wang, L., Zhang, L., 2019. Endophyte infection enhances accumulation of organic acids and minerals in rice under Pb 2+ stress conditions. Ecotoxicol. Environ. Saf. 174, 255–262. https://doi.org/10.1016/j.ecoenv.2019.02.072.

Li, W., Erickson, E.M., Manthiram, A., 2020. High-nickel layered oxide cathodes for lithium-based automotive batteries. Nat. Energy 5, 26–34. https://doi.org/10.1038/s41560-019-0513-0.

Melaku, S., Dams, R., Moens, L., 2005. Determination of trace elements in agricultural soil samples by inductively coupled plasma-mass spectrometry: microwave acid digestion versus aqua regia extraction. Anal. Chim. Acta 543, 117–123. https://doi.org/10.1016/j.aca.2005.04.055.

Moreno-García, A.F., Neri-Torres, E.E., Mena-Cervantes, V.Y., Altamirano, R.H., Pineda-Flores, G., Luna-Sánchez, R., García-Solares, M., Vazquez-Arenas, J., Suastes-Rivas, J.K., 2021. Sustainable biorefinery associated with wastewater treatment of Cr (III) using a native microalgae consortium. Fuel 290. https://doi.org/10.1016/j.fuel.2020.119040.

Mudd, G.M., Jowitt, S.M., Werner, T.T., 2017. The world's lead-zinc mineral resources: scarcity, data, issues and opportunities. Ore Geol. Rev. 80, 1160–1190. https://doi.org/10.1016/j.oregeorev.2016.08.010.

Novotny, Z., Mulakaluri, N., Edes, Z., Schmid, M., Pentcheva, R., Diebold, U., Parkinson, G.S., 2013. Probing the surface phase diagram of Fe3O4(001) towards the fe-rich limit: evidence for progressive reduction of the surface. Phys. Rev. B: Condens. Matter Mater. Phys. 87, 1–8. https://doi.org/10.1103/PhysRevB.87.195410.

Opitz, M.W., Daneshkhah, R., Lorenz, C., Ludwig, R., Steinkellner, S., Wieczorek, K., 2021. Serendipita indica changes host sugar and defense status in Arabidopsis thaliana: cooperation or exploitation? Planta 253, 74. https://doi.org/10.1007/s00425-021-03587-3.

Peng, C., Chen, S., Shen, C., He, M., Zhang, Y., Ye, J., Liu, J., Shi, J., 2018. Iron plaque: a barrier layer to the uptake and translocation of copper oxide nanoparticles by rice plants. Environ. Sci. Technol. 52, 12244–12254. https://doi.org/10.1021/acs.est.8b02687.

Peng, Y., Yan, Y., Wang, J., Xiang, Z., Li, Y., Yang, J., Yin, J., Wang, W., Xiao, H., 2022. CdSe cluster-modified biogenic α-FeOOH based on macroporous biochar for Fenton-like reaction of As(III). Appl. Surf. Sci. 589, 152872. https://doi.org/10.1016/j.apsusc.2022.152872.

Robinson, M., Oshlack, A., 2010. A scaling normalization method for differential expression analysis of RNA-seq data. Genome Biol. 11, R25. https://doi.org/10.1186/gb-2010-11-3-r25.

Rozpądek, P., Domka, A., Ważny, R., Nosek, M., Jędrzejczyk, R., Tokarz, K., Turnau, K., 2018. How does the endophytic fungus Mucor sp. improve Arabidopsis arenosa vegetation in the degraded environment of a mine dump? Environ. Exp. Bot. 147, 31–42. https://doi.org/10.1016/j.envexpbot.2017.11.009.

Rozpądek, P., Nosek, M., Domka, A., Ważny, R., Jędrzejczyk, R., Tokarz, K., Pilarska, M., Niewiadomska, E., Turnau, K., 2019. Acclimation of the photosynthetic apparatus and alterations in sugar metabolism in response to inoculation with endophytic fungi. Plant Cell Environ. 42, 1408–1423. https://doi.org/10.1111/pce.13485.

Rueda, H., Arenas, M., Vargas-Balda, R., Blanco, S., Delvasto, P., 2021. Production of a nickel-based catalyst for urea electrooxidation using spent batteries as raw material: electrochemical synthesis and implications from a circular economy stand-point. Sustain. Mater. Technol. 29. https://doi.org/10.1016/j.susmat.2021.e00296.

Sahrawat, K.L., 2004. Iron toxicity in wetland rice and the role of other nutrients. J. Plant Nutr. 27, 1471–1504. https://doi.org/10.1081/PLN-200025869.

Saifuddin, N., Wong, C.W., Yasumira, A.A.N., 2009. Rapid biosynthesis of silver nanoparticles using culture supernatant of bacteria with microwave irradiation. E-J.Chem. 6, 61–70. https://doi.org/10.1155/2009/734264.

Saslowsky, D.E., Dana, C.D., Winkel-Shirley, B., 2000. An allelic series for the chalcone synthase locus in Arabidopsis. Gene 255, 127–138. https://doi.org/10.1016/S0378-1119(00)00304-8.

Scott, B., Takemoto, D., Tanaka, A., 2007. Fungal endophyte production of reactive oxygen species is critical for maintaining the mutualistic symbiotic interaction between Epichloë festucae and perennial ryegrass. Plant Signal. Behav. 2, 171–173. https://doi.org/10.4161/psb.2.3.3725.

St-Cyr, L., Fortin, D., Campbell, P.G.C., 1993. Microscopic observations of the iron plaque of a submerged aquatic plant (Vallisneria americana Michx). Aquat. Bot. 46, 155–167. https://doi.org/10.1016/0304-3770(93)90043-V.

Stumm, W., Blber, M.V., 1994. An in-situ ATR-FTIR study: the surface coordination of salicylic acid on aluminum and iron(III) oxides. Environ. Sci. Technol. 28, 763–768. https://doi.org/10.1021/es00054a004.

Tanaka, A., Christensen, M.J., Takemoto, D., Park, P., Scott, B., 2006. Reactive oxygen species play a role in regulating a fungus-perennial ryegrass mutualistic interaction. Plant Cell 18, 1052–1066. https://doi.org/10.1105/tpc.105.039263.

Tropf, S., Lanz, T., Rensing, S.A., Schröder, J., Schröder, G., 1994. Evidence that stilbene synthases have developed from chalcone synthases several times in the course of evolution. J. Mol. Evol. 38, 610–618. https://doi.org/10.1007/BF00175881.

Tropf, S., Karcher, B., Schroder, G., Schroder, J., 1995. Reaction mechanisms of homodimeric plant polyketide synthases (stilbene and chalcone synthase). A single active site for the condensing reaction is sufficient for synthesis of stilbenes, chalcones, and 6'-deoxychalcones. J. Biol. Chem. 270, 7922–7928. https://doi.org/10.1074/jbc.270.14.7922.

Vadassery, J., Ranf, S., Drzewiecki, C., Mithöfer, A., Mazars, C., Scheel, D., Lee, J., Oelmüller, R., 2009. A cell wall extract from the endophytic fungus Piriformospora indica promotes growth of Arabidopsis seedlings and induces intracellular calcium elevation in roots. Plant J. 59, 193–206. https://doi.org/10.1111/j.1365-313X.2009.03867.x.

Vahabi, K., Sherameti, I., Bakshi, M., Mrozinska, A., Ludwig, A., Reichelt, M., Oelmüller, R., 2015. The interaction of Arabidopsis with Piriformospora indica shifts from initial transient stress induced by fungus-released chemical mediators to a mutualistic interaction after physical contact of the two symbionts. BMC Plant Biol. 15, 58. https://doi.org/10.1186/s12870-015-0419-3.

Vainshtein, M., Belova, N., Kulakovskaya, T., Suzina, N., Sorokin, V., 2014. Synthesis of magneto-sensitive iron-containing nanoparticles by yeasts. J. Ind. Microbiol. Biotechnol. 41, 657–663. https://doi.org/10.1007/s10295-014-1417-4.

Vilgalys, R., Hester, M., 1990. Rapid genetic identification and mapping of enzymatically amplified ribosomal DNA from several Cryptococcus species. J. Bacteriol. 172, 4238–4246. https://doi.org/10.1128/jb.172.8.4238-4246.1990.

Ważny, R., Rozpądek, P., Jędrzejczyk, R.J., Śliwa, M., Stojakowska, A., Anielska, T., Turnau, K., 2018. Does co-inoculation of Lactuca serriola with endophytic and arbuscular mycorrhizal fungi improve plant growth in a polluted environment? Mycorrhiza 28, 235–246. https://doi.org/10.1007/s00572-018-0819-y.

Ważny, R., Rozpądek, P., Domka, A., Jędrzejczyk, R.J., Nosek, M., Hubalewska-Mazgaj, M., Lichtscheidl, I., Kidd, P., Turnau, K., 2021a. The effect of endophytic fungi on growth and nickel accumulation in Noccaea hyperaccumulators. Sci. Total Environ. 768. https://doi.org/10.1016/j.scitotenv.2020.144666.

Ważny, R., Rozpądek, P., Jędrzejczyk, R.J., Domka, A., Nosek, M., Kidd, P., Turnau, K., 2021b. Phytohormone based biostimulant combined with plant growth promoting endophytic fungus enhances Ni phytoextraction of Noccaea goesingensis. Sci. Total Environ. 789. https://doi.org/10.1016/j.scitotenv.2021.147950.

Xu, D., Fan, D., Shen, W., 2013. Catalyst-free direct vapor-phase growth of Zn1-xCuxO microcross structures and their optical properties. Nanoscale Res. Lett. 8, 1–9. https://doi.org/10.1186/1556-276X-8-46.

Zhang, Z.Q., Shu, W.S., Lan, C.Y., Wong, M.H., 2001. Soil seed bank as an input of seed source in revegetation of lead/zinc mine tailings. Restor. Ecol. 9, 378–385. https://doi.org/10.1046/j.1526-100X.2001.94007.x.

Zhang, Q., Chen, H., Xu, C., Zhu, H., Zhu, Q., 2019. Heavy metal uptake in rice is regulated by pH-dependent iron plaque formation and the expression of the metal transporter genes. Environ. Exp. Bot. 162, 392–398. https://doi.org/10.1016/j.envexpbot.2019.03.004.

Zheng, R.-L., Cai, C., Liang, J.-H., Huang, Q., Chen, Z., Huang, Y.-Z., Arp, H.P.H., Sun, G.-X., 2012. The effects of biochars from rice residue on the formation of iron plaque and the accumulation of Cd, Zn, Pb, As in rice (Oryza sativa L.) seedlings. Chemosphere 89, 856–862. https://doi.org/10.1016/j.chemosphere.2012.05.008.

Zielonka, A., Klimek-Ochab, M., 2017. Fungal synthesis of size-defined nanoparticles. Adv. Nat. Sci. Nanosci. Nanotechnol. 8. https://doi.org/10.1088/2043-6254/aa84d4.

Zinicovscaia, I., Yushin, N., Grozdov, D., Vergel, K., Ostrovnaya, T., Rodlovskaya, E., 2020. Metal removal from complex copper containing effluents by waste biomass of Saccharomyces cerevisiae. Ecol. Chem. Eng. S 27, 415–435. https://doi.org/10.2478/eces-2020-0027.